Geochemistry of molybdenum in the continental crust

Allison T Greaney, Roberta L Rudnick, Richard M Gaschnig, Joseph B Whalen, Béatrice Luais, John D Clemens

Elsevier Editorial System(tm) for Geochimica et Cosmochimica Acta

Manuscript Draft

Manuscript Number: GCA-D-17-00802R3

Title: Geochemistry of Molybdenum in the Continental Crust

Article Type: Article

Corresponding Author: Ms. Allison T. Greaney,

Corresponding Author's Institution: University of California Santa Barbara

First Author: Allison T. Greaney

Order of Authors: Allison T. Greaney; Roberta L Rudnick; Richard M Gaschnig; Joseph B Whalen; Beatrice Luais; John D Clemens

Abstract: The use of molybdenum as a quantitative paleo-atmosphere redox sensor is predicated on the assumption that Mo is hosted in sulfides in the upper continental crust (UCC). This assumption is tested here by determining the mineralogical hosts of Mo in typical Archean, Proterozoic, and Phanerozoic upper crustal igneous rocks, spanning a compositional range from basalt to granite. Common igneous sulfides such as pyrite and chalcopyrite contain very little Mo (commonly below detection limits of around 10 ng/g) and are not a significant crustal Mo host. By contrast, volcanic glass and Ti-bearing phases such as titanite, ilmenite, magnetite, and rutile contain significantly higher Mo concentrations (e.g., up to 40 µg/g in titanite), and can account for the whole-rock Mo budget in most rocks. However, mass balance between whole-rock and mineral data is not achieved in 4 out of 10 granites analyzed with in-situ methods, where Mo may be hosted in undetected trace molybdenite. Significant Mo depletion (i.e., UCC-normalized Mo/Ce < 1) occurs in nearly every granitic rock analyzed here, but not in oceanic basalts or their differentiates (Greaney et al., 2017; Jenner and O'Neill, 2012). On average, granites are missing ~60% of their expected Mo contents. There are two possible reasons for this: 1) Mo partitions into an aqueous magmatic vapor/fluid phase that is expelled from cooling plutons, and/or 2) Mo is partitioned into titaniferous phases during partial melting and fractional crystallization of an evolving magma. The first scenario is likely given the high solubility of oxidized Mo. However, correlations between Mo/Ce and Nb/La in several plutonic suites suggest fractionating phases such as rutile or Fe-Ti oxides may sequester Mo in lower crustal rocks or in subducting slabs in arc settings.

Geochemistry of Molybdenum in the Continental Crust

Allison T. Greaney[1,2]*, Roberta L. Rudnick[1,2], Richard M. Gaschnig[1,3], Joseph B. Whalen[4], Béatrice Luais[5], John D. Clemens[6]

[1]University of Maryland College Park, Department of Geology, College Park, MD 20742

[2]*present address:* University of California Santa Barbara, Department of Earth Science and Earth Research Institute, Santa Barbara, CA, USA 93106

[3]*present address:* University of Massachusetts Lowell, Department of Environmental, Earth, and Atmospheric Science, Lowell, MA, USA 01854

[4]Geological Survey of Canada, Central Canada Division, Ottawa, Ontario, Canada K1A0E8

[5]Centre de Recherches Pétrographiques et Géochimiques – CRPG, CNRS - UMR 7358, Université de Lorraine, 54501 Vandoeuvre-les-Nancy Cedex, France

[6]Stellensbosch University, Department of Earth Sciences, Matieland, 7600 South Africa

*corresponding author: greaney@umail.ucsb.edu

Abstract

The use of molybdenum as a quantitative paleo-atmosphere redox sensor is predicated on the assumption that Mo is hosted in sulfides in the upper continental crust (UCC). This assumption is tested here by determining the mineralogical hosts of Mo in typical Archean, Proterozoic, and Phanerozoic upper crustal igneous rocks, spanning a compositional range from basalt to granite. Common igneous sulfides such as pyrite and chalcopyrite contain very little Mo (commonly below detection limits of around 10 ~~ppb~~ng/g) and are not a significant crustal Mo host. By contrast, volcanic glass and Ti-bearing phases such as titanite, ilmenite, magnetite, and rutile contain significantly higher Mo concentrations (e.g., up to 40 µg/g in titanite), and can account for the whole-rock Mo budget in most rocks. However, mass balance between whole-rock and mineral data is not achieved in 4 out of 10 granites analyzed with *in-situ* methods, where Mo may be hosted in undetected trace molybdenite. Significant Mo depletion (i.e., UCC-

normalized Mo/Ce < 1) occurs in nearly every granitic rock analyzed here, but not in oceanic basalts or their differentiates (Greaney et al., 2017; Jenner and O'Neill, 2012). On average, granites are missing ~60% of their expected Mo contents. There are two possible reasons for this: 1) Mo partitions into an aqueous magmatic vapor/fluid phase that is expelled from cooling plutons, and/or 2) Mo is partitioned into titaniferous phases during partial melting and fractional crystallization of an evolving magma. The first scenario is likely given the high solubility of oxidized Mo. However, correlations between Mo/Ce and Nb/La in several plutonic suites suggest fractionating phases such as rutile or Fe-Ti oxides may sequester Mo in lower crustal rocks or in subducting slabs in arc settings.

1. Introduction

Molybdenum (Mo) geochemistry has emerged as a powerful tool for tracking early atmospheric oxygenation (e.g., Anbar et al., 2007; Wille et al., 2007; Gaschnig et al., 2014), redox conditions in ocean basins (e.g., Siebert et al., 2003; Arnold et al., 2004; Scott et al., 2008; Dahl et al., 2011), and the influence of subducted sediments and fluids on arc magmas (Freymuth et al., 2015; König et al., 2016). The interest in Mo stems from its geochemical properties: Mo is a multi-valent element whose partitioning behavior depends on the redox state of its environment. Despite the rapidly growing literature on the geochemical behavior of Mo at Earth's surface, the behavior of Mo in igneous rocks is less well understood. Yet, such knowledge is crucial for understanding how Mo will behave during crustal weathering and processes that release Mo to sedimentary environments. Additionally, determining the mineralogical hosts of Mo in evolving magmas will lead to a more accurate understanding of Mo behavior during crust formation and differentiation, and the formation of molybdenite deposits in

various tectonic settings. This task was first undertaken by Kuroda and Sandell (1954) but, with improved methodology, we aim to expand upon their dataset.

1.1 Properties of Mo

Molybdenum is a geochemically versatile element that displays siderophile (iron/metal-loving; Kuroda and Sandell, 1954; Newsom and Palme, 1984; Lodders and Palme, 1991; Walker, 2016), chalcophile (Goldschmidt, 1937; Kuroda and Sandell, 1954), and lithophile behavior (rock/silicate-loving; Newsom and Palme, 1984; Greaney et al., 2017), depending on the composition of the system of interest (including fO_2 and fS_2), the temperature, and the pressure. Molybdenum's redox sensitivity plays a prominent role in its geochemical behavior because its charge, size, and physical properties change depending on its oxidation state. Molybdenum is insoluble in aqueous fluids when reduced to its tetravalent state, but when oxidized to its hexavalent state it becomes soluble. This relationship between charge and solubility is a key factor in determining the behavior of Mo in the crust and on the Earth's surface.

In igneous systems, the transition from Mo^{4+} to Mo^{6+} occurs over a span of ~10 log units fO_2 (O'Neill and Eggins, 2002), with Mo^{4+} being the dominant state at around three log units below the IW buffer (iron-wüstite) and Mo^{6+} being the dominant state at around one log unit below the FMQ buffer (fayalite-magnetite-quartz). Thus, Mo is expected to exist in its oxidized state in mantle and crustal melts, which have oxygen fugacities near the fayalite-magnetite-quartz (FMQ) or Ni-Ni-oxide (NNO) buffers. The work of Fitton (1995), Zack et al (2002), and subsequent experimental studies suggest that Mo partitions into rutile in eclogites (eclogitic rutile: 2-7 µg/g ~~ppm~~ Mo; Zack et al., 2002), and can be removed from melts generated in subduction zones, even though Mo is found predominately as 6+ in oxidized experimental melts

(Holzheid et al., 1994; O'Neill and Eggins, 2002; Bali et al., 2012; Skora et al. 2017). Bali et al. (2012) show that Mo is compatible in rutile in oxidized systems at the NNO buffer (nickel-nickel oxide). This suggests that Mo may be incorporated into rutile even in its oxidized state. Octahedrally-coordinated Mo^{6+} has a similar ionic radius to octahedrally-coordinated Ti^{4+} (59 and 60.5 pm, respectively; Shannon, 1976), so it can replace Ti in a coupled substitution to maintain electrical neutrality. Alternatively, Mo may be locally reduced to Mo^{4+} (ionic radius = 60.5 pm) before exchanging for Ti^{4+} in an isovalent substitution (Zack et al., 2002; Skora et al. 2017). It has also been proposed that Mo is predominately hosted in biotite and amphibole in igneous rocks (Voegelin et al., 2014; Yang et al., 2017), supporting the idea that it follows similar substitution patterns as Ti. However, Mo can also be reduced and incorporated into molybdenite (MoS_2) during oxidation-reduction reactions that occur in hydrothermal ore systems (Stein, 1985).

On the surface of Earth and in oceans, 'free' Mo exists in its oxidized, soluble state given the abundance of atmospheric O_2. Unreactive molybdate (MoO_4^{2-}) is the most common form of Mo in rivers and oceans today, where Mo has a residence time of around 440,000 years (Miller et al., 2011). However, this was probably not the case on early Earth, which lacked or contained only trace concentrations of atmospheric oxygen.

1.2 Molybdenum as a redox proxy

Throughout the first ~ 2 billion years of Earth's history, the atmosphere was far more reducing than today, probably containing $< 10^{-5}$ times the present atmospheric level (PAL) of O_2 (Kasting, 2014 and references therein). Atmospheric oxygen did not accumulate to significant levels until the Great Oxidation Event (GOE), which occurred between 2.4 Ga and 2.3 Ga, when

93 it likely rose to somewhere between 10^{-4} and 10^{-2} PAL (Lyons et al, 2014 and references
94 therein).

95 Many lines of evidence point to the rise of O_2 during the GOE. Arguably the most
96 important is the disappearance of sulfur-isotope mass-independent fractionation, caused by the
97 creation of an atmospheric ozone shield (Farquhar et al., 2000). Additionally, several redox-
98 sensitive metal proxies (Mo, U, Cr, Re) indicate that oxidative weathering of the continents
99 commenced at or just before the GOE, suggesting that atmospheric O_2 had become sufficiently
100 abundant to cause oxidative weathering of crustal rocks (Anbar et al, 2007; Wille et al., 2007;
101 Scott et al., 2008). These redox-sensitive metals are assumed to be concentrated in minerals that
102 will break down in the presence of atmospheric oxygen, *i.e.*, in sulfides in the case of Mo. Pyrite
103 and molybdenite are commonly invoked as the main Mo sources that contain reduced, insoluble
104 Mo (Anbar et al., 2007, Miller et al., 2011). When these sulfides break down in the presence of
105 atmospheric O_2, the Mo becomes oxidized (and thereby soluble), and can be transported in
106 solution as molybdate (MoO_4^{2-}) in rivers, and eventually the oceans. Once in the ocean, Mo is
107 slowly removed through uptake by Fe-Mn oxides in oxygenated environments, or deposited in
108 black shales within euxinic (high-S, low-O_2) environments. Archean and Proterozoic black
109 shales have been analyzed for Mo and other redox-sensitive elements to track oxidative
110 continental weathering; enrichments suggest oxidative weathering and/or the development of
111 euxinic ocean basins (Turekian and Bertine, 1971; Helz, 1996; Erickson and Helz, 2000). High
112 sulfur concentrations are required in the water column for Mo to be reduced and incorporated
113 into Fe-Mo-S phases in reduced oceanic sediments (Helz, 1996; Erickson and Helz, 2000). Like
114 Mo, sulfur was probably not abundant in the Archean oceans until atmospheric oxygen caused
115 weathering of continental sulfides during the GOE (Canfield, 2005).

As observed by Gaschnig et al. (2014), Mo enrichments in black shales during and after the GOE are accompanied by contemporaneous Mo depletions in the UCC. The UCC Mo depletion, relative to the light rare earth elements of similar compatibility (Ce and Pr) first appears in the Paleoproterozoic and continues to the present day. These observations support the hypothesis that oxidative weathering of the continents played a role in removing Mo from the weathered continental crust and transporting it into ocean basins after the GOE.

The use of Mo to trace atmospheric O_2 and infer Precambrian oceanic chemistry is widely accepted in the paleo-atmospheric research community. However, using the Mo concentrations in euxinic sediments to quantify the pO_2 is based on the assumption that Mo is primarily concentrated in sulfides in the UCC, and that these sulfides will break down at a rate that is proportional to pO_2 (Anbar et al., 2007; Williamson and Rimstidt, 1994). While Mo may behave as a chalcophile element in euxinic sedimentary and low-temperature hydrothermal environments, its behavior during igneous differentiation and crust formation is less well understood. Newsom and Palme (1984) suggested that Mo will behave incompatibly during mantle melting, like Ce and Pr, and this is corroborated by the observation that Mo is significantly enriched in the UCC (1.1 µg/g~~ppm~~; Rudnick and Gao, 2003) relative to the primitive mantle (0.039 to 0.047 µg/g~~ppm~~; Greber et al., 2015 and Palme and O'Neill, 2004, respectively). Moreover, Mo is observed to behave incompatibly during differentiation of intraplate basalt magmas (Yang et al., 2015; Greaney et al., 2017). Greaney et al. (2017) also showed that while Mo is present in magmatic sulfides (average 2.6 µg/g~~ppm~~), it is more abundant in basaltic to andesitic volcanic glasses (average 5 µg/g~~ppm~~) and Fe-Ti oxides (average 6.4 µg/g~~ppm~~). However, the partitioning behavior of Mo in typical continental crustal igneous rocks, such as granites, has not been systematically studied.

Here, we explore the partitioning of Mo in typical UCC granitic rocks, and incorporate data published on Hawaiian basalts (Greaney et al., 2017), to determine whether Mo is chalcophile, *i.e.*, concentrated primarily in sulfides in the igneous UCC. We present *in-situ* data on Mo concentrations in various minerals as well as whole-rock data on Mo abundances in granitic and basaltic rocks. Our goals are to determine the main mineralogical hosts of Mo in the continental crust and to improve our understanding of the behavior of Mo during crust formation and differentiation.

2. Samples

Granitic rocks are considered to be representative of the felsic UCC, so granitic rocks that span Earth's history form the focus of this study. Since Mo is thought to be generally incompatible during igneous differentiation (Newsom and Palme, 1984), it is expected to be concentrated in more felsic rocks. Given the bimodal composition of the crust, and the hypothesis that the Archean crust may have been significantly more mafic than present-day UCC (e.g., Taylor and McLennan, 1985; Condie, 1993; Dhuime et al., 2015; Gaschnig et al., 2016; Tang et al., 2016), partitioning data from Hawaiian basalts (Greaney et al., 2017) and MORB (Jenner and O'Neill, 2012; Patten et al., 2013) are also considered. We were particularly interested in sampling Archean crust, because its Mo residence and weathering behavior is directly applicable to the GOE. When possible, we selected granitic rocks that retained igneous textures and mineralogy, with an aim of studying previously well-characterized samples. Archean and Proterozoic samples come from the Superior Province (Whalen et al., 2002; Whalen et al., 2003), Baffin Island (Whalen et al. 2012), the Zimbabwe craton (Luais and Hawkesworth, 1994), and the Barberton greenstone belt (Clemens et al. 2006). The majority of these samples are TTGs (tonalite-trondjhemite-granodiorite rocks) that contain higher sodium

contents than the more potassic granites that dominate the Proterozoic and Phanerozoic. Additionally, due to the presence of residual rutile or ilmenite in lower-crustal residues and amphibole in mid-crustal residues (Hoffmann et al. 2011), TTG's are generally characterized by a depletion in the high field-strength elements (HFSE) Ti, Nb, and Ta. Complete sample descriptions and photomicrographs can be found in the supplementary materials.

2.1 Barberton TTGs (3.55 – 3.21 Ga)

Powdered samples of TTGs from the Barberton Greenstone Terrane were analyzed here for whole-rock compositions. No thin sections were available for *in-situ* work. Samples from four generations of plutons that represent distinct tectono-magmatic events were studied: the 3.55-3.49 Ga Steynsdorp pluton; the 3.46-3.42 Ga Stolzburg, Doornhoek, Theespruit, and Erstehoek plutons; the 3.29-3.24 Ga Badplaas pluton; and the 3.24-3.23 Ga Nelshoogte pluton (Clemens et al., 2006; Moyen et al., 2007; Kröner et al., 1991). The Barberton Terrane is one of the most intensively studied suites of Archean TTGs in the world, and several interpretations have been developed to explain the petrogenesis of the TTGs and greenstone belts. A consensus has developed around the hypothesis that these plutons were emplaced during accretion of an exotic terrane and subsequent post-orogenic collapse (Clemens et al., 2006; Moyen et al., 2007).

2.2 Superior Province TTGs (3.0 – 2.7 Ga)

The TTGs from the Superior Province come from the North Caribou Terrane plutonic complex (~3.0 Ga; Whalen et al., 2003) and the Central Wabigoon sub-province (~2.7 Ga; Whalen et al., 2002). The North Caribou samples are mainly derived from the English Lake Plutonic Suite and range in composition from felsic tonalites and trondhjemites to amphibolitic and pyroxenitic xenolithic enclaves that may have originated as cumulates. Geochemical modeling suggests a genetic link between the cumulate enclaves and the TTGs, and an overall

hydrous source for this suite. The younger Central Wabigoon samples are classified as granite to granodiorite and have a higher K_2O/Na_2O ratios than the North Caribou TTGs. This suite is thought to have formed from the partial melting of over-thickened lower crust during the collision of arcs, such as the one that potentially produced the North Caribou samples. Both whole-rock and *in-situ* data were collected for this suite. Three samples were sectioned for *in-situ* analysis. These are composed of quartz, plagioclase, K-feldspar, biotite, amphibole (primarily hornblende), titanite, Fe-Ti oxides, and minor muscovite and sulfides (Fig. 1), all of which were analyzed for Mo concentration.

2.3 Zimbabwe Craton TTGs (2.9 – 2.6 Ga)

The samples from the Zimbabwe craton are mainly tonalites from the 2.9 Ga Mashaba suite, as well as two samples from the 2.6 Ga Chibi Granite. The Zimbabwe craton is bounded by three belts that accreted between the Neoarchean Limpopo Belt and the Neoproterozoic Zambezi and Mozambique Belts. The craton itself is composed of 2.8 – 2.5 Ga greenstone sequences and 3.5 – 2.9 Ga TTGs. Luais and Hawkesworth (1994, 2002) outline a petrogenetic model that involves partial melting of a garnet-bearing amphibolite and subsequent fractional crystallization to produce the TTG suites. In this model, the Mashaba tonalite was formed by direct fusion products of basaltic proto-lower crust leaving a garnet amphibolite residue. The late Chibi granite is interpreted to have been derived through partial melting of greenstone mafic volcanic rocks (Hawkesworth et al., 1979). Partial melting in the deeper part of a thick crust has been invoked to explain the formation of these units (Hawkesworth et al., 1979; Luais and Hawkesworth, 1994 and 2002). Whole-rock and *in-situ* data were collected for this suite, and data for major and trace elements were previously published in Luais and Hawkesworth (1994). The four samples selected for *in-situ* analysis are variably foliated and contain alteration

products such as chlorite, cummingtonite, epidote, and sericite. Common phases are quartz, plagioclase, K-feldspar, biotite, hornblende, muscovite, titanite, Fe-Ti oxides, apatite, and zircon.

2.4 Baffin Island (1.88 Ga)

Whole-rock powders from the Qikiqtarjuaq Plutonic Suite (QPS) show the largest compositional range of all suites studied here, varying from granodiorite/tonalite to gabbro (Whalen et al., 2012). These intrusive bodies form a portion of the Cumberland batholithic complex on Baffin Island. The origin of the QPS is uncertain, as it is a relatively newly discovered and analyzed unit. However, U-Pb ages suggest that it is ~35 Myr older than the Cumberland Batholith (Rayner et al., 2012), which has been interpreted to be a Trans-Hudson Orogeny post-accretionary batholith, possibly resulting from a delamination event from the base of over-thickened crust (Whalen et al., 2010). Thus, it can be inferred that the QPS was emplaced at the initiation of an accretionary event, and may be arc-derived. Data for all major and trace elements were previously published in Whalen et al. (2012), but Mo concentrations were re-analyzed in this study using a more precise standard-addition technique. No thin sections were analyzed.

2.5 Phanerozoic Granites

Mesozoic granitic rocks from the Western USA (Gaschnig et al., 2011; 2017) and a Silurian granite from the Eastern US were analyzed as well. These include a garnet-bearing peraluminous granite from the Idaho batholith, a metaluminous tonalite from the Lookout Mountain pluton in the Blue Mountains (Oregon and Idaho, USA), and a Neo-Acadian epidote-bearing granodiorite (Ellicott City Granodiorite, Maryland, USA). These samples consist of common granitic minerals – abundant feldspar, quartz, biotite, and amphibole with accessory muscovite, titanite, epidote, magnetite, ilmenite, apatite, allanite, zircon, and sulfides (Fig. 1, see supplementary

231 sample descriptions). Whole-rock and *in-situ* analyses of thin sections were carried out on these
232 samples.

233 *2.6 Kilauea Iki lavas*

234 Data from the Kilauea Iki lava lake, Hawaii, reported in Greaney et al. (2017), are
235 considered here for a more complete assessment of mineralogical hosts of Mo. The lava lake
236 erupted in 1959 and is considered a prime natural laboratory for studying basaltic magma
237 differentiation. Samples ranging through the entire differentiation suite from 43.7 to 57.1 wt%
238 SiO_2 were subjected to whole-rock and *in-situ* analysis. The rocks contain olivine, pyroxene
239 (augite), plagioclase, Fe-Ti oxides, glass, and minor apatite and sulfides (Fig. 1).

240 **3. Methods**

241 The methods follow those of Greaney et al. (2017) and Gaschnig et al. (2015), and are
242 reproduced here in detail in the supplementary material. Whole-rock trace element analyses were
243 carried out by standard-addition solution inductively coupled plasma mass spectrometry (ICP-
244 MS). Samples were dissolved in high pressure PTFE bombs using HF/HNO3, then three aliquots
245 were spiked with variable known amounts of Mo using spikes created by Gaschnig et al. (2015).
246 This method produces a calibration curve from the sample itself, instead of having to extrapolate
247 a calibration curve from external standards, which could induce errors associated with the
248 extrapolation and improperly calibrated standards. The sample aliquots were analyzed on an
249 Element2 HR-ICP-MS at the University of Maryland in MR and LR mode for three isotopes of
250 Mo (95, 97, and 98). The limit of detection (LOD) ranged from 0.03 µg/g~~ppm~~ to 0.10 µg/g~~ppm~~
251 for most analytical sessions. However, it was as high as 0.16 µg/g~~ppm~~ during analyses of the
252 Barberton suite TTGs. The variable LOD is reflected in Table 1. The reported Mo abundances
253 for the three isotopes never varied by more than the reported RSD calculated from the counting

254 statistics. USGS standard reference rock powders AGV-2 and BHVO-1 were dissolved alongside
255 each batch of samples and run as secondary standards (Table 2). AGV-2's external
256 reproducibility results in a 2RSD of 7%. BHVO-1 (2RSD ~ 25%) is notoriously difficult to
257 reproduce (Willbold et al., 2016; Gaschnig et al. 2015), possibly due to heterogeneities in the
258 sample powder.
259 In addition, to demonstrate the robustness of measuring low-Mo abundances with the
260 standard addition method, three low-[Mo] TTGs from different suites were re-dissolved and
261 analyzed by isotope dilution at the Arizona State University Keck Biogeochemistry Lab. Two of
262 the three samples show excellent reproducibility, while the isotope-dilution data gave even lower
263 Mo abundances for the third sample, ZB89-10 (0.13 µg/g~~ppm~~ by ID vs. 0.25 µg/g ~~ppm~~ by
264 standard addition). This discrepancy may reflect a slightly heterogeneous powder due to nuggets
265 of a Mo-rich phase, given that mass balance was not achieved for this sample (see section 4.1.3
266 and Table S4), and a Mo-rich phase was observed within magnetite of another sample from this
267 same TTG suite (see section 4.1.1). These replicate data are reported in the online supplement.
268 Additionally, for most plutonic suites, a full suite of trace elements were analyzed, including Ga,
269 Ge, Cd, In, Sn, Sb, W, Tl, and Bi. These data are provided in the supplementary materials.
270 *In-situ* mineral data were collected using electron probe microanalysis (EPMA) followed
271 by laser ablation ICP-MS using a New Wave UP-213 nm laser attached to an Element2 HR-ICP-
272 MS at the University of Maryland and a Photon Machines 193 nm laser attached to an Agilent
273 7700x Quadropole ICP-MS at the University of California Santa Barbara. NIST-610 was the
274 external standard, and the glasses BHVO-2g and NIST-612, as well as a synthetic Mo-bearing
275 sulfide produced by James Brenan (formerly at the University of Toronto, now at Dalhousie
276 University) were analyzed as secondary standards (Table 2). Spot-sizes ranged from 25 µm (for

277 smaller sulfides) to 80 µm (for silicates and larger sulfides). Three isotopes of Mo were
278 measured (95, 97, and 98), with all returning values that fell within the error calculated by
279 counting statistics, except when an obvious interference was present (e.g., $^{55}Mn^{40}Ar$ on ^{95}Mo in
280 garnet). Abundances of ^{98}Mo are therefore reported for the *in-situ* data. The LOD for *in-situ* Mo
281 analyses ranges were typically ~0.01 µg/g~~ppm~~, however they occasionally ranged as high as 0.1
282 µg/g~~ppm~~, depending on the analyte/background ratio of the instrument that day. The LA-ICP-
283 MS data were processed using Iolite (Paton et al. 2011).

284 **4. Results**

285 *4.1 In-situ data*

286 4.1.1 Sulfides

287 A total of 78 sulfide grains were analyzed from the Phanerozoic granites, TTGs, and several
288 evolved samples from the Kilauea Iki lava lake, Hawaii. Pyrite, chalcopyrite, and pyrrhotite are
289 present in the granitic samples while the sulfide blebs in the Kilauea Iki lavas form solid
290 solutions between isocubanite and bornite (see Greaney et al., 2017 for analyses). The sulfides
291 are volumetrically insignificant (<1 vol. %) in all of the analyzed samples, and, for most
292 samples, did not register in mineral modes determined by point counting (see the mass balance
293 table in the supplement).

294 Molybdenum concentrations (designated as [Mo]) in accessory sulfides vary by
295 approximately three orders of magnitude (0.01 µg/g~~ppm~~ to 9.2 µg/g~~ppm~~). The maximum [Mo] is
296 found in the Kilauea Iki lava-hosted sulfides (mean $[Mo]_{Kilauea\ sulfides}$ = 2.7 µg/g~~ppm~~, max = 9.2
297 µg/g~~ppm~~) while the granite-hosted sulfides contain significantly less Mo than those from Kilauea
298 Iki (mean $[Mo]_{granite\ sulfides}$ = 0.72 µg/g~~ppm~~, max = 8.0 µg/g~~ppm~~, Fig. 2), but have similar
299 concentrations to MORB-hosted sulfides (Patten et al., 2013). Molybdenite was not found as an

accessory phase in any sample, but one grain of magnetite in a TTG from the Zimbabwe craton (ZB89-53) contains significant Mo (~1300 µg/g~~ppm~~), along with Pb and other chalcophile elements. This suggests that a small nugget of MoS_2, or similar phase, may have been embedded within or beneath the magnetite grain, but was not visible on the surface. This analysis was excluded from the magnetite data presented in Fig. 2 and Table 3**.**

4.1.2 Silicates and Oxides

In addition to sulfides, quartz, K-feldspar, plagioclase, biotite, muscovite, hornblende, titanite, garnet, allanite, zircon, epidote, chlorite, olivine, clinopyroxene (augite), volcanic glass, magnetite, ilmenite, rutile, and the rare accessory phase columbite (also called niobite) were all analyzed for their Mo abundances (Table 3). The mean data presented in this table also include analyses that were below the LOD in plagioclase, K-feldspar, biotite, amphibole, muscovite, sulfides, epidote, and quartz. In these cases, the lower LOD commonly calculated for these analyses (0.01 µg/g ~~=ppm~~) was used to calculate the mean [Mo] value. Thus, the average concentrations for these phases should be considered maxima. Collectively, these data encompass nearly every major mineral found in common igneous rocks. Most phases were analyzed repeatedly across several rock types and localities except for columbite/niobite, which is confined to a single crystal in a Phanerozoic granite (07RMG52).

Molybdenum concentrations are presented in box and whisker plots in Figure 2 with the phases arranged from highest to lowest [Mo], as established by the median [Mo] value. Molybdenum concentrations are considered to be significant if they are greater than 1 µg/g~~ppm~~ (average UCC [Mo] = 1.1 µg/g~~ppm~~; Rudnick and Gao, 2014). Titanite consistently contains significant Mo, except for one sample from the Superior Province (WXP99-176), in which titanite contained between 0.01 and 0.5 µg/g~~ppm~~. Metamorphic rutile replaced part of the titanite

in that sample and may have preferentially incorporated Mo into its lattice, removing it from the titanite. Excluding this sample, [Mo] in titanite is commonly >30 µg/g~~ppm~~. Ilmenite and magnetite are the other two common phases that routinely contained ≥ 1 µg/g~~ppm~~ Mo in both granitic and basaltic samples. Rutile and columbite/niobite are less common upper crustal minerals, but they were found as primary igneous and secondary metamorphic assemblages in some samples and contain significant Mo. Volcanic glass was also found to be a significant host of Mo in the Kilauea samples where the average Mo_{glass} concentration is 4.8 µg/g~~ppm~~. Glass data from ~600 MORB samples (Jenner and O'Neill, 2012) are shown for comparison, and have an average [Mo] of 0.62 µg/g~~ppm~~, which is significantly lower than KI glass because MORB has lower whole-rock [Mo], and many of the KI lavas are more evolved than MORB. Most of the minerals analyzed do not contain abundant (>1 µg/g~~ppm~~) Mo, including the most common minerals in granitic and basaltic rocks: quartz, feldspars, biotite, amphibole, olivine, and pyroxenes. Sulfides are found near the middle or right-hand side of each plot in Fig. 2, reflecting their generally low [Mo], relative to other minerals. Sulfide data from MORB (Patten et al., 2013) are shown for comparison to OIB sulfides on the plot of basaltic minerals.

4.1.3 Mass Balance

Mineral modes were determined for the samples using a least-squares regression program, MINSQ (Herrmann and Berry, 2002). Select samples were also point counted to ensure accuracy of the MINSQ program (supplementary materials). The modal abundances are used together with the measured Mo concentrations to calculate the primary location of Mo (Fig. 3; mass balance provided in supplementary materials). Given their scarcity, sulfides were not registered in point counting exercises, so they were assigned modal abundances of 0.01% to 0.1%, which are likely to be overestimates in most samples. Nevertheless, in most samples the sulfide [Mo] contributes

346 less than 3% of the whole-rock [Mo]. The maximum sulfide Mo contribution occurs in the
347 Kilauea Iki volcanic rocks, where sulfides contain up to 6% of the total whole-rock [Mo]. By
348 contrast, titaniferous phases are the dominant hosts of Mo in granitic rocks. Silicates can also
349 contribute a significant portion of the total Mo budget (e.g., ~25% in one sample, Fig 3), given
350 their volumetric significance in granites. The calculated Mo distribution results in $[Mo]_{\text{whole rock, calculated}}$ that can be compared to measured whole rock data and $[Mo]_{\text{whole rock, measured}}$, to see if a
352 mass balance is attained.

353 Given analytical uncertainties on the standard addition, laser ablation, and modal mineralogy
354 measurements, we consider that mass balance is achieved if the calculated whole-rock
355 abundance is within 20% of the measured whole-rock value. Of the ten granitic samples
356 evaluated, mass balance is attained in only six. The remaining four are missing anywhere
357 between 60 and 80% of the expected Mo abundance, based-on the whole-rock [Mo] measured by
358 standard addition ICP-MS. All thin sections were carefully examined to ensure that no phase was
359 missing from *in-situ* analysis. The incomplete mass balance is probably a real phenomenon, and
360 is discussed further below.

361 *4.2 Whole-rock data*

362 Whole-rock [Mo] data are presented in Table 1 and a complete dataset, including major and
363 trace elements (including Ga, Ge, Cd, In, Sn, Sb, W, Tl, and Bi), is presented in the online
364 supplement. Almost all granitic rocks analyzed contain less than 1 µg/g~~ppm~~ Mo, except for three
365 samples from Baffin Island. Several Kilauea Iki samples (data presented in Greaney et al., 2017)
366 contain more than 1 µg/g~~ppm~~ because they are derived from an enriched mantle source and
367 evolved further than most MORB, without Mo fractionation on a whole-rock scale.

368 4.2.1 Data representation

During mantle melting and igneous differentiation, Mo is expected to have similar partitioning behavior to the LREE, specifically Ce and Pr given their comparable ionic radii (Newsom and Palme, 1984). Therefore, Mo concentrations are plotted between these two elements on modified multi-element plots (Fig. 4) that have been normalized to the upper continental crust values of Rudnick and Gao (2014). In addition to LREE, Nb is included to indicate whether a sample has a Nb depletion (UCC normalized Nb/La < 1) that may be induced by Ti-oxide fractionation in the subducting slab or during differentiation. The majority of analyzed granitic rocks analyzed are depleted in Mo, relative to Ce and Pr. Only nine of the 45 samples show either a smooth LREE-Mo profile with no depletion, or are enriched in Mo. Given the normalized values for Ce and Pr, an expected Mo value (Mo*) can be calculated as $([Ce]_n \times [Pr]_n)^{0.5}$ where "n" means normalized to the UCC value of Rudnick and Gao (2015). The percentage of Mo "missing" from a given sample can then be calculated as $100 \times (Mo^* - Mo_{meas})/Mo^*$. Between 20 and 90% (with a mean of 60%) of Mo is missing from the 36 samples that show Mo depletion, which equates to between 0.04 and 2.0 ~~μg/gppm~~, depending on the sample. Details regarding the Mo* calculation can be found in the supplement.

5. Discussion

5.1 Mineralogical Hosts of Mo

In igneous rocks, Mo is not primarily hosted in accessory sulfide minerals such as pyrite, pyrrhotite, and chalcopyrite. This is most probably due to the relatively oxidized nature of magmas, in which Mo exists in its hexavalent state (O'Neill and Eggins, 2012), making the formation of MoS_2 rare. We conclude that Mo does not behave as a chalcophile element in primary magmatic settings, because it is not sufficiently reduced to be incorporated into a sulfide phase without the presence of abundant reduced sulfur. This contrasts with the behavior of Mo in

392 the low-T epithermal systems that are commonly associated with pluton cooling, in which Mo^{6+}
393 is reduced by H_2S in the exsolving fluids to form molybdenite (Hannah et al., 2007).
394 The most important Mo-bearing phases in the igneous rocks analyzed here are titanite
395 ($[Mo]_{mean}$ = 15.9 µg/g~~ppm~~), magnetite ($[Mo]_{mean}$ = 5.83 µg/g~~ppm~~), ilmenite ($[Mo]_{mean}$ = 4.09
396 µg/g~~ppm~~), and glass ($[Mo]_{mean}$ = 4.83 µg/g~~ppm~~) (Fig. 2). Columbite ($FeNb_2O_6$) is also a
397 significant Mo host in one sample from the Idaho batholith, but this is an uncommon mineral. As
398 pointed out above, octahedrally coordinated Mo^{6+} has a similar ionic radius to octahedrally
399 coordinated Ti^{4+} (73 and 74.5 pm, respectively; Shannon, 1976), which occurs in ilmenite,
400 titanite, and rutile. Likewise, the ionic radius of tetrahedral Mo^{6+} is similar to tetrahedral Ti^{4+} (55
401 and 56 pm, respectively), which occurs in pseudobrookite (a common oxide mineral in the KI
402 lavas) and other titaniferous spinel-group minerals. A coupled substitution with a divalent cation
403 is needed to maintain electrical neutrality when hexavalent Mo replaces tetravalent Ti. This
404 could be achieved by substitution of Fe^{2+} (ionic radius of 75 pm) into octahedrally coordinated
405 sites. In pseudobrookite, for example, an additional mole PFU of Fe^{2+} replacing Fe^{3+} for each
406 mole of Mo replacing Ti would satisfy charge balance.
407 Other minor Mo hosts include silicates such as garnet ($[Mo]_{mean}$ = 0.33 µg/g~~ppm~~) and
408 biotite ($[Mo]_{mean}$ = 0.15 µg/g~~ppm~~). These results generally agree with those of Voegelin et al.
409 (2014) who found that biotite has the highest Mo abundance of any silicate analyzed in their
410 study, which also included analyses of feldspars, hornblende, olivine, and pyroxenes
411 ($[Mo]_{biotite,Voegelin}$=0.67 µg/g~~ppm~~), while feldspars contained less than 0.1 µg/g~~ppm~~. Although
412 these silicates have low Mo concentrations, their high volumetric abundances may contribute
413 significantly to total crustal Mo abundances, as up to 25% of the total whole-rock Mo is
414 attributed to silicates in one tonalite from the Superior Province (Fig. 3). Moreover, these phases

415 are relatively easily altered, compared to the titaniferous phases, and will act as a source of Mo
416 during continental weathering.

417 Molybdenite (MoS_2) was not observed in any of the samples analyzed here, but we propose
418 that very small grains of MoS_2 could complete the mass balance in some samples. While it is
419 relatively rare for it to occur as an accessory phase in granites, molybdenite, which contains 60%
420 Mo by weight, is a highly-concentrated source of Mo in the crust, and occurs as a fairly common
421 ore mineral that forms during epithermal processes associated with the emplacement of granitic
422 plutons. Since it is so Mo-rich, an exceedingly small 'nugget' of MoS_2 (e.g., <0.0004 vol. % of a
423 thin section) could complete the mass balance in samples that show deficits between calculated
424 and measured whole-rock [Mo]. While uncommon, MoS_2 inclusions in quartz have been
425 documented in felsic igneous rocks (Audétat et al., 2011). The role of MoS_2 in the overall Mo
426 budget of the crust, as well as the weathering properties of all Mo-bearing phases, are discussed
427 further in sections 5.2.2 and 5.2.3.

428 *5.2 Mo behavior during magmatic differentiation*

429 5.2.1 Mo depletion in granites

430 Depletion of Mo relative to Ce and Pr is observed in every granitic suite analyzed here, with
431 most of the samples (36 out of 45) exhibiting Mo depletion. The depletion is evident whether the
432 data are normalized to primitive mantle (McDonough and Sun, 1995) or UCC values (Rudnick
433 and Gao, 2014), and is especially stark when compared to MORB and Kilauea Iki data, in which
434 Mo has a similar or higher normalized abundance to the LREE (Fig. 4), as predicted by Newsom
435 and Palme (1984). Additionally, recently published Mo data for granites from the Lachlan Fold
436 Belt also show an UCC-normalized Mo depletion in the majority of samples for which published
437 Ce data could be located (Yang et al., 2017, and references therein). The widespread depletion of

Mo in granitic rocks may be due to the following two processes, which are not mutually exclusive: a) Mo could be lost from an evolving magma to a fractionating titaniferous phase such as rutile or Fe-Ti oxides (Kuroda and Sandell, 1954; Fitton, 1995; Audétat et al., 2011), or b) Mo could be lost to a magmatic vapor phase (MVP) exsolved from a cooling pluton (Candela and Holland, 1984; Audétat, 2010; Audétat et al., 2011). We also propose that S-type granites may show Mo depletion because their source (detrital sediments from oxidatively weathered sources) are depleted in Mo (per Gaschnig et al., 2014). However, with the exception of sample 07RMG52, the granitic rocks analyzed here are not proper S-type granites as determined by mineralogy and Aluminum Saturation Index, so this hypothesis does not apply to our data. The hypothesis that Mo is removed during crystal fractionation/accumulation in residual phases is evaluated by determining whether Mo depletion correlates with Nb depletion in the pluton suites, while MVP exsolution is evaluated by examining correlations between Mo and other fluid-soluble elements.

5.2.2 Hypothesis 1: Loss of Mo due to partitioning into titaniferous phases

Within this first hypothesis, we propose two processes that may inhibit Mo from reaching the upper crust: 1) Mo-loss could be due to fractionation of titaniferous phases (e.g., ilmenite, magnetite, rutile, titanite) during igneous differentiation, and/or, 2) In arc settings, Mo could be retained in residual rutile in a subducting slab, like Nb. These are both likely explanations for the Mo depletion given the observed affinity that Mo has for rutile (Fitton, 1995; Zack et al., 2002) and other Ti-bearing phases like ilmenite and magnetite (Arnorsson and Oskarsson, 2006; Audétat, 2010; Greaney et al., 2017; this study), and they are not mutually exclusive. Titanite, a major host of Mo in most of the titanite-bearing samples analyzed here, could also potentially play a role in removing Mo and Nb as well (Marks et al., 2008), although it crystallizes relatively

late in a cooling magma. A correlation between Mo/Ce and Nb/La is observed in several of the plutonic suites analyzed here (Fig. 5), suggesting that fractionation into Fe-Ti oxides during differentiation may remove these elements from an evolving magma. This process may sequester Mo and Nb in lower- or mid-crustal cumulates.

The Baffin Island Qikiqtarjuaq Plutonic Suite is an excellent example of differentiation from gabbro to granite. It exhibits a strong correlation between Mo/Ce and Nb/La ($R^2 = 0.92$, Fig 5) suggesting that Mo and Nb share the same geochemical behavior as the magma evolved. All Baffin Island samples have an UCC-normalized Nb/La ratio <1, suggesting that Nb was initially sequestered in rutile during subduction and mantle melting. The differentiation suite also displays a negative correlation between Nb and SiO_2 ($R^2 = 0.81$) and a negative correlation between Mo/Ce and SiO_2 ($R^2 = 0.75$) over a range from 50.3 to 72.3 wt% SiO_2, suggesting that both elements were removed by crystal fractionation, instead of behaving incompatibly (Fig. S2). In this plutonic suite, Nb was most likely held in residual rutile, and was then further sequestered in fractionating Fe-Ti oxides, along with Mo, during differentiation (Figs. 4 and 5). The Mo enrichments in the more mafic to intermediate samples may reflect an overabundance of these Mo-bearing minerals relative to the more evolved rocks. This decrease in Mo with differentiation contrasts with observations of Mo increase during differentiation at Hekla volcano, Iceland (Yang et al., 2015) and at Kilauea Iki, Hawaii (Greaney et al., 2017). There appears to be a correlation between Mo/Ce and Nb/La in the Superior Province samples as well (Fig. 5, R^2=0.89), although this strong correlation is achieved by ignoring an apparent outlier in the data. The Mashaba tonalities from the Zimbabwe Craton show a much weaker correlation between Nb/La and Mo/Ce (R^2=0.34) and Ti/Gd and Mo/Ce (R^2=0.42). However, it should be noted that the degree of differentiation in the Zimbabwe tonalites is much less than that observed in other

484 samples and that these samples have been interpreted to represent nearly pure partial melts of a
485 basaltic source without significant fractional crystallization (Luais and Hawkesworth, 1994).
486 Nevertheless, there is a strong correlation between Nb/Ta and SiO_2 in the Zimbabwe data,
487 suggesting that a Ti-bearing phase (e.g., titanite) is being removed from this system during
488 differentiation, but either is not taking Mo with it, or the fractionation signature is overprinted by
489 another process (Fig. S3). We have insufficient data on Phanerozoic granites to draw conclusions
490 about magmatic differentiation for those samples.
491 Molybdenum isotope studies also support the hypothesis that Mo is partitioned into
492 fractionating Ti-bearing phases. Based on the data in Voegelin et al. (2014), Yang et al. (2017)
493 propose that sequestration of Mo-bearing phases (they suggest biotite and hornblende) in the
494 lower crust may explain the heavy δ^{98}Mo isotope signature observed in UCC rocks relative to
495 basalts. Additionally, Wille et al. (2018) suggest that Mo isotopes may be fractionated during
496 crystallization of amphibole or clinopyroxene in arc settings. Overall, a net isotope fractionation
497 is observed between average UCC felsic rocks (~ +0.15‰; Willbold and Elliott, 2017) and
498 MORB (~ 0.0‰; Liang et al., 2017; Bezard et al., 2016) and OIB (~ -0.14‰; Liang et al., 2017),
499 suggesting that not only [Mo] but also Mo isotopes may be fractionated during igneous
500 differentiation (Voegelin et al., 2014; Yang et al., 2017; Liang et al., 2017; Greber et al., 2015;
501 Wille et al., 2018). By contrast, other studies show that Mo abundances and isotopes are not
502 significantly fractionated by differentiation processes in intraplate and arc settings (Yang et al.
503 2015; Gaschnig et al., 2017).
504 Alternatively, many researchers have proposed that Mo abundances (Fitton, 1995) and
505 isotopes may be fractionated during dehydration and partial melting of the subducting slab in arc
506 settings (Willbold and Elliott, 2017; König et al., 2008). Specifically, Fitton (1995) observed that

507 a coupled Mo and Nb depletion in arc magmas may represent sequestration of these elements in
508 rutile in the subducting slab. Experimental work of Bali et al. (2012) found that at the Ni-NiO
509 buffer, Mo is retained in rutile relative to slab fluids, adding credence to this hypothesis. While
510 sulfides are not found to be major hosts of Mo in granites, Skora et al. (2017) demonstrated
511 experimentally that sulfides and rutile can fractionate Mo during sediment/slab melting in a
512 subduction zone, given sufficiently reducing conditions. This study did not measure Mo
513 abundances in the sulfides or rutile, so partition coefficients are unknown. However, Zack et al.
514 (2002) found that Mo is significantly enriched in rutile relative to sulfide minerals in eclogites
515 and therefore conclude that sulfides contribute less than 5% of the total eclogite Mo budget.
516 Audétat (2010) suggested that Mo may be sequestered in monosulfide solid solution (MSS)
517 during partial melting (e.g., of slab/sediment) and igneous differentiation, given the measured
518 $D^{MSS/melt} \sim 80$. However, a recent study of sulfide-saturated arc lavas found no Mo depletion after
519 the onset of sulfide saturation during differentiation (Jenner, 2017). Instead, Mo is seemingly
520 enriched in the resulting sulfide-depleted magmas. Further studies of Mo in magmatic
521 differentiation suites and in subduction zones are needed to determine which exact phase/s, if
522 any, is/are responsible for elemental and isotopic fractionation.

523 5.2.3 Hypothesis 2: Mo loss during fluid exsolution

524 As outlined by Audétat (2010) and Audétat et al. (2011), it is likely that Mo is lost from
525 granites due to exsolution of aqueous magmatic fluids or vapor phases, because experimental
526 studies show that Mo is partitioned into these phases (Candela and Holland, 1984; Zajacz et al.,
527 2017). Partition coefficients ($D^{fluid/melt}$) vary due to the nature of different ligands (e.g., Cl, F) and
528 salinity, but typically range from D = 1 to D = 20 (Zajacz et al., 2008). Molybdenum loss during
529 aqueous fluid exsolution would probably lead to the saturation of molybdenite (MoS_2) in

530 epithermal veins surrounding the plutons and, on larger scales, formation of economically viable
531 Mo porphyry deposits.
532 Some TTG suites show only a weak (e.g., Zimbabwe, Fig. 5) or no correlation (e.g.,
533 Barberton) between Mo and Nb or Mo and Ti, which suggests that fractionation of Mo by Ti- or
534 Nb-bearing phases did not play a dominant role in the evolution of the Mo budgets of these
535 magmas. Alternatively, fractionation may not be captured by the limited differentiation range in
536 these TTGs. Nevertheless, these plutonic suites (except for one set of Barberton TTGs) still show
537 significant Mo depletion. In the Zimbabwe suite, Mo is variably correlated with Cs ($R^2 = 0.84$),
538 Sb ($R^2 = 0.73$), Pb ($R^2 = 0.56$), and As ($R^2 = 0.46$) (Fig. S4) all of which are moderately
539 compatible in a low-salinity fluid phases (Zajacz et al., 2008), and these elements are known to
540 be expelled from granitic plutons. However, several of these correlations hinge on a single data
541 point (Fig. S4). There is no correlation between these fluid-mobile elements and incompatible,
542 less-fluid mobile elements such as the LREE, implying that the fluid-mobile element
543 concentrations are dominated by processes other than crystal-melt differentiation. Indeed, Mo is
544 more strongly depleted relative to Ce in this suite of TTGs relative to other locales (lower Mo/Ce
545 ratio in Fig. 5), so a vapor phase may have preferentially removed Mo from the Zimbabwe
546 TTGs. In contrast to the Zimbabwe samples, no individual pluton suite displays convincing ($R^2 >$
547 0.4) multi-element correlations in the Barberton TTGs. Correlations between Mo and fluid-
548 soluble elements are also not found for the Superior Province or Baffin Island samples. Thus, we
549 suggest that different processes of Mo-loss from plutons (fluid exsolution v. crystal
550 fractionation) may be acting on different plutonic suites, and these processes are not mutually
551 exclusive.

If we explore the hypothetical end-member case in which the effects of crystal fractionation are assumed to be negligible, and Mo behaves as an incompatible element in all systems, then loss through fluid exsolution to form MoS_2 could account for all calculated Mo depletions. In this scenario, it can be inferred that approximately 60% (average Mo lost from a pluton – see supplement information on Mo* calculation) of the Mo in un-weathered UCC granites is hosted in MoS_2. This is a maximum estimate, because it is likely that Mo loss from the magma during partial melting or crystal fractionation also occurs.

A simple calculation can be used to estimate the maximum amount of Mo released from plutons to form molybdenite. We start with the following parameters and assumptions: the continental crust covers 210×10^6 km^2 of the Earth's surface (Cawood et al., 2013) and, to a depth of 10 km, 40% of that area is granitic rock that initially contains 0.5 µg/g~~ppm~~ Mo (the average interpolated Mo abundance, Mo*, of this study). Mean Mo loss from the granites in this study is 60%, and we initially assume that all Mo 'lost' is due to vapor-phase partitioning. With these assumptions, a maximum 10^{14} kg of Mo would have been released from UCC granitic plutons to form MoS_2. If we instead assume that granite only composes 20% of the upper 10 km of the crust, and only 10% of the Mo missing from a pluton is a result of MoS_2 formation, then approximately 10^{13} kg of Mo would have been released from UCC granitic rocks to form MoS_2. Thus, we conclude that a maximum of 10^{13} kg to 10^{14} kg of Mo may be hosted in MoS_2 in the upper 10 km of the continental crust. The USGS has identified ~10^{10} kg of Mo resources available for mining (rounding to the nearest order of magnitude) (USGS, 2009). This suggests that up to three to four orders of magnitude more Mo may lie inaccessible beneath the surface of the continental crust.

574 In summary, a combination of fractionation during differentiation and loss via vapor phase
575 exsolution probably contributes to the total Mo loss recorded in granites. This would explain
576 discrepancies between plutonic suites – among which some show strong Ti-mineral fractionation
577 signatures and others do not – yet, nearly all of the samples studied here show depletions in total
578 [Mo]. Further studies of magmatic suites formed by partial melting with Fe-Ti oxides in the
579 residue, or differentiation involving fractionation of Fe-Ti oxides are needed to test these
580 hypotheses.

581 *5.3 Release of Mo during oxidative weathering of the UCC*

582 Mo enrichments in black shales that form in euxinic (S-rich) ocean basins are first
583 observed in the rock record at around 2.5 Ga and persist through the Phanerozoic, with a second
584 period of increased Mo abundances beginning at the end of the Proterozoic (Anbar et al. 2007;
585 Scott et al., 2008; Wille et al., 2007). These enrichments are interpreted to reflect changing
586 atmospheric and oceanic oxidation states due to the GOE and the Neoproterozoic Oxidation
587 Event. However, before Mo concentrations in black shales can be calibrated as a paleo-
588 atmospheric oxybarometer, one must first know which O_2 sensitive mineral phases host Mo in
589 the continental crust (Anbar et al., 2007). We have shown here that molybdenite, specifically, is
590 the predominant sulfide host of Mo in the UCC, while other common magmatic sulfides and
591 their subsolidus exsolution products (pyrite, chalcopyrite, etc.) do not contain significant Mo.
592 Based on our findings, it is likely that Mo released from MoS_2 during oxidative weathering is the
593 source of Mo enrichment observed in oceanic sediments since the GOE. Thus, experimentally-
594 determined oxidation rates of MoS_2 at low pO_2 are needed to derive the pO_2 of the atmosphere
595 during the GOE (e.g., Greber et al., 2015). While authigenic pyrite may host some Mo in
596 sedimentary rocks (e.g., Gregory et al., 2017), Mo must first be removed from the primary

igneous crust before it can be concentrated in these phases. If Mo was not released significantly from the igneous UCC prior to the GOE – which is likely given the lack of Mo depletion in pre-GOE diamictites (Gaschnig et al., 2014) – then authigenic sulfides were probably not a weatherable source of Mo from the continental crust at the time of the GOE.

Given the strength of the Ti-O bond, titaniferous phases are fairly resistant to weathering, so Mo will not be easily released from them, irrespective of pO_2. It is very likely that Mo remains in these minerals as the source rocks are weathered and the titaniferous minerals are incorporated into sediments as detrital minerals. However, Mo is also highly enriched in volcanic glass – a phase that is susceptible to weathering in anoxic and oxic environments. Therefore, we propose that weathering of volcanic glass may have released Mo from the crust before the rise of atmospheric oxygen. As no Mo depletion is observed in the UCC before the GOE (Gaschnig et al., 2014), this process was probably not widespread on the continents. However, soluble Mo^{6+} may have been released into the pre-GOE oceans from submarine weathering of glassy basalt. This Mo might have been immediately reduced and sequestered if sufficient S, or another reductant, existed in the water column. Alternatively, if there was insufficient S in the water column to reduce Mo prior to the GOE (as suggested by Canfield, 2005), Mo might have remained in solution in pre-GOE oceans and is therefore not recorded in the marine rock record. This hypothesis has implications for the timing of the evolution of Mo-co-factored enzymes that fix nitrogen, as sufficient Mo must be present in the water column for it to be incorporated into these enzymes (Stüeken et al., 2015). However, this assumes that Mo is not immediately reduced once it is weathered out of volcanic glass, and that Mo is not hosted in secondary alteration phases. Both of these assumptions need to be tested with weathering models and analyses of Mo in altered basalts.

620 *5.4 Molybdenum enrichments in rift-related magmas*

621 The Barberton Terrane is composed of TTGs, greenstones (metamorphosed Archean basaltic
622 rocks), and sedimentary units that were formed between 3.5 and 3.2 Ga. The samples studied
623 here span 300 Myr in age and were formed during three to four distinct tectono-magmatic events
624 at 3.5 Ga, 3.46 Ga, 3.29 Ga and 3.24 Ga (Clemens et al., 2006, Kröner et al., 1991). On the basis
625 of field relationships and pluton geochemistry, Moyen et al. (2006) interpreted the terrane to
626 have formed during collision of exotic blocks (3.55 – 3.42 Ga plutons) followed by a main
627 orogenic event (3.25 – 3.21 Ga) during which the Badplaas pluton was emplaced. This was
628 followed by post-orogenic collapse at 3.22 – 3.21 Ga, contemporaneous with emplacement of the
629 Nelshoogte pluton in an extensional setting. The plutonic suites emplaced during accretion and
630 the main orogenic stage exhibit Mo depletions relative to LREE (with the exception of one
631 sample from the Stolzburg pluton, STZ), while the Nelshoogte (NLG) pluton, which is
632 associated with post-orogenic collapse, is not depleted in Mo (Fig. 6). The concentrations of
633 REE do not change significantly between the different suites, but the NLG plutonic suite is less
634 enriched in LREE relative to HREE, and is slightly more magnesian. This observation that Mo is
635 enriched in ~3.2 Ga rift-related magmas is similar to Mo-enrichments observed in rift-related
636 magmas today.

637 Similarly, while many economic Mo deposits are associated with arc-derived, calc-alkaline
638 magmas (Westra and Keith, 1981; Whalen et al., 2001), the highest-grade Mo-porphyry deposits
639 are associated with rift settings (e.g., Climax-type deposits; Ludington and Plumlee, 2009), and
640 alkaline magmas from continental rifts show significant Mo enrichments (Audétat, 2010;
641 Audétat et al., 2011). The source of Mo in these rift-related magmas is unclear; both the
642 lithospheric mantle and the continental crust have been suggested as sources. Sun et al. (2016)

propose that assimilation of sedimentary rocks enriched in Mo (e.g., black shales) may be the source of Mo. Other researchers have suggested that the Mo may ultimately be sourced from Mo-enriched mantle melts that undergo fractional crystallization (Audétat, 2010; Pettke et al., 2010). Pettke et al. (2010) proposed that the lithospheric mantle may be re-enriched in Mo through subduction-related metasomatism, and that alkaline magmas may be generated from this Mo-rich reservoir during rifting events.

The observation that Mo is enriched in the ~3.2 Ga rift-related NLG pluton can be used to test these hypotheses. Significant Mo enrichments in black shales only occur after the onset of widespread oxidative weathering at ~2.4 Ga (Scott et al., 2008; Anbar et al., 2007). Thus, the hypothesis that rift magmas assimilate Mo-rich sediments, proposed by Sun et al. (2016) does not hold for these Archean magmas. There is evidence for subduction-related magmatism in the Barberton suite (Moyen et al., 2006; Furnes et al., 2012), which adds credence to the hypothesis that a subducting slab may have enriched the lithospheric mantle in Mo (Pettke et al., 2010). However, this hypothesis remains contentious because many authors argue that subduction zones mainly arose after 3.2 Ga (e.g., Condie and Kröner, 2008; Tang et al., 2016, and references therein).

In the Barberton samples, Mo correlates with Ni (Fig. 7a) and Cr (Fig. 7b**)**. Additionally, the overall Mo enrichment of the NLG pluton relative to LREE resembles that of MORB and Hawaiian lavas (Fig. 4), suggesting a mafic, *i.e.*, mantle, origin for the Mo. Lithospheric mantle-derived Mo is a something of a paradox because the lithospheric mantle is refractory and should be depleted in incompatible Mo. This paradox could be resolved if the lithospheric mantle were metasomatized with fluids derived from a subducting slab, and then partially melted during a subsequent rifting event (Pettke et al., 2010). Alternatively, it is possible that the Mo enrichments

may be derived from partial melting of Mo-rich cumulates (e.g., Fe-Ti oxides and rutile bearing rocks such as amphibolites and eclogites) during continental rifting. In this scenario, lower crustal rocks may contain the missing Mo recorded in granitic suites and explain the origin of the Mo enrichment in various rift-related magmatic suites. This hypothesis implies that sequestration of Mo in Fe-Ti oxides in lower crustal cumulates must be significant, and further analyses of Mo abundances in such rocks are needed to evaluate this idea.

Conclusions

- In 'common' UCC granitic rocks, Mo is hosted primarily in weathering-resistant, titaniferous phases such as titanite, ilmenite, and magnetite, while in basaltic to andesitic volcanic rocks, Mo is predominately hosted in ilmenite, magnetite, and interstitial glass. Molybdenum mass balance based on in situ analyses of Mo in silicates and oxides cannot be completed in a few granitic samples, suggesting nuggets of MoS_2 may be a significant Mo host in some felsic plutonic rocks.
- Silicates (e.g., quartz, biotite, and amphibole) generally contain less than 0.2 µg/g~~ppm~~ Mo, but may be volumetrically significant hosts, contributing up to 25% of the whole-rock Mo in one granitic rock analyzed here.
- Common accessory phase sulfides (e.g., pyrite, chalcopyrite, immiscible sulfide blebs) are not significant hosts of Mo in granitic or basaltic rocks.
- Nearly all analyzed granitic rocks are depleted in Mo (by 20 – 90%, mean = 60%), relative to Ce and Pr. This may reflect MoS_2 precipitation from fugitive magmatic vapor phases or loss of Mo to fractionating Ti- and Nb-bearing phases during slab melting or magmatic differentiation. Some plutonic suites show correlations between Mo and Nb, suggesting loss of Mo due to fractionation of Fe-Ti oxides or other titaniferous phases. Other plutonic suites

Comment [RLR1]: You mention titanite in the response to reviews.

show correlations between Mo and fluid-soluble elements (e.g., Cs, Pb, As, etc), potentially pointing to Mo loss in an aqueous magmatic vapor phase.

- If all Mo lost from granitic rocks is attributed to aqueous fluid exsolution and subsequent MoS_2 precipitation, then, on average, 60% of the Mo budget in a pluton would have to be concentrated in distal, epithermal veins that crystallized MoS_2. This is most likely an overestimate as it represents the endmember scenario where all Mo is lost through vapor-phase fractionation.
- The ~3.2 Ga rift-related Nelshoogte pluton from the Barberton Greenstone Belt is the only group of samples studied here that do not show a systematic Mo depletion. This is similar to observations of Mo-enrichments in modern rift-related magmas. These data can be used to rule out the hypothesis that Mo enrichments in rift-related magmas are derived from melting of Mo-rich sediments like black shales, because Mo was not enriched in black shales prior to the GOE at ~2.4 Ga. If subduction was occurring at this time, subduction-related metasomatism of the lithospheric mantle could be the source of the enrichment in Mo in these rift-related magmas (Pettke et al., 2010). Alternatively, mantle melts generated during rifting may have assimilated Mo-rich residues in the lower crust or upper mantle to create these Mo enrichments in rift-related magmas. This would imply that significant Mo is removed from evolving magmas in Fe-Ti oxides. Further analyses of Mo in differentiated suites and lower crustal cumulates are needed to test this hypothesis.
- The processes of Mo-loss through fluid/vapor-phase partitioning or fractionation of titaniferous phases are likely not mutually exclusive. Here we present arguments for the two end-member scenarios but emphasize that further research is needed to determine the proportion of Mo-loss by these two processes.

Comment [RLR2]: I think you need to name it here so that people understand that it is not all of the Barberton samples that don't show Mo depletion.

Acknowledgements

We thank Aleisha Johnson, George Helz, Gary Stevens, and Scott Wipperfurth for valuable discussions, Richard Ash, Phil Piccoli, and Andrew Kylander-Clark for analytical assistance, and Steve Romaniello for assistance in reproducing the whole-rock data in the ASU Keck Lab for Biogeochemistry. We also thank the three reviewers (Thomas Ulrich, and two anonymous reviewers) for their suggestions that helped us to improve the paper. The work was supported by a National Science Foundation grant EAR 133810 (A. Anbar, PI; R.L. Rudnick, co-I), EAR 1757313, and the University of Maryland.

References

Anbar A.D., Duan Y., Lyons T.W., Arnold G.L., Kendall B., Creaser R.A., Kaufman A.J., Gordon G.W., Scott C., Garvin J., Buick R. (2007) A Whiff of Oxygen Before the Great Oxidation Event?, *Science* **317**, 1903-1906

Arnold, G. L., Anbar, A. D., Barling, J., & Lyons, T. W. (2004). Molybdenum isotope evidence for widespread anoxia in mid-proterozoic oceans, *Science* **304**, 87–90.

Arnorsson S. and Oskarsson N. (2006) Molybdenum and tungsten in volcanic rocks and in surface and <100 °C ground waters in Iceland, *Geochim Cosmochim Acta* **71**, 284-304

Audétat A. (2010) Source and Evolution of Molybdenum in the Porphyry Mo (-Nb) Deposit at Cave Peak, Texas, *J. Petrol.* **51**, 8, 1739-1760

Audétat A., Dolejs D., Lowenstern J.B. (2011) Molybdenite Saturation in Silicic Magmas: Occurrence and Petrological Implications, *J. Petrol*. **52**, 5, 891-904

Bali E., Keppler H., Audetat A. (2012) The mobility of W and Mo in subduction zone fluids and the Mo-W-Th-U systematics of island arc magmas, *Earth Planet Sci. Lett.* **351-352**, 195-207

734 Bezard R., Fischer-Godde M., Hamelin C., Brennecka G.A., Kleine T. (2016) The effects of
735 magmatic processes and crustal recycling on the molybdenum stable isotopic composition of
736 Mid-Ocean Ridge Basalts, *Earth Planet Sci. Lett.* **453**, 171-181
737 Candela P.A. and Holland H.D. (1984) The partitioning of copper and molybdenum between
738 silicate melts and aqueous fluids, *Geochim Cosmochim Acta*, **48**, 373-380
739 Canfield D.E. (2005) The early history of atmospheric oxygen: Homage to Robert M. Garrels,
740 *Annu. Rev. Earth Planet. Sci,* **33**, 1-36
741 Cawood P.A., Hawkesworth C.J., Dhuima B. (2013) The continental record and the generation
742 of the continental crust, *GSA Bull.* **125**, 14-32
743 Clemens J.D., Yearron L.M., Stevens G. (2006) Barberton (South Africa) TTG magmas:
744 Geochemical and experimental constraints on source-rock petrology, pressure of formation
745 and tectonic setting, *Precambrian Res.* 1**51**, 53-78
746 Condie K.C. (1993) Chemical composition and evolution of the upper continental crust:
747 Contrasting results from surface samples and shales, *Chem. Geol*. **104**, 1-37
748 Condie and Kröner (2008) When did plate tectonics begin? Evidence from the geologic record,
749 *GSA Special Paper*, **440**, 281-294
750 Dahl T.W., Canfield D.E., Rosing M.T., Frei R.E., Gordon G.W., Knoll A.H., Anbar A.D.
751 (2011) Molybdenum evidence for expansive sulfidic water masses in ~750 Ma oceans,
752 *Earth Planet Sci. Lett.* **311**, 264-274
753 Dhuime B., Wuestefeld A., Hawkesworth C.J. (2015) Emergence of modern continental crust
754 about 3 billion years ago, *Nature Geoscience* **8**, 552-555
755 Erickson B.E. and Helz G.R. (2000) Molybdenum(VI) speciation in sulfidic waters: Stability and
756 lability of thiomolybdates, *Geochim. Cosmochim. Acta* **64**, 1149-1158

757 Farquhar J., Bao H., Thiemens M. (2000) Atmospheric Influence of Earth's Earliest Sulfur
758 Cycle, *Nature* **289**, 756-758
759 Fitton, J.G. (1995) Coupled molybdenum and niobium depletion in continental basalts, *Earth*
760 *Planet Sci. Lett.* **136**, 715-721
761 Freymuth H., Vils F., Willbold M., Taylor R., Elliot T. (2015) Molybdenum mobility and
762 isotopic fractionation during subduction at the Mariana arc, *Earth Planet Sci. Lett.* **432**, 176-
763 186
764 Furnes H., Robins B., De Wit M.J. (2012) Geochemistry and petrology of lavas in the upper
765 Onverwacht suite, Barberton Mountain Land, South Africa. *S. Af. J. Geol*. **115** 171-210
766 Gaschnig R.M., Macho A.S., Fayon A., Schmitz M., Ware B.D., Vervoort J.D., Kelso P.,
767 LaMaskin T.A., Kahn T.J., Tikoff B. (2017) Intrusive and depositional constraints on the
768 Cretaceous tectonic history of the southern Blue Mountains, eastern Oregon, *Lithosphere* **9**,
769 265-282
770 Gaschnig R. M., Reinhard C. T., Planavsky N. J., Wang X., Asael D., Chauvel C. (2017). The
771 molybdenum isotope system as a tracer of slab input in subduction zones: An example from
772 Martinique, Lesser Antilles Arc. *Geochem. Geophys. Geosyst.* **18**, 4674–4689
773 Gaschnig R.M., Rudnick R.L., McDonough W.F., Kaufman A.J., Valley J.W., Gao S., Beck M.
774 (2016) Compositional evolution of the upper continental crust through time, as constrained
775 by ancient glacial diamictites, *Geochim. Cosmochim. Acta* **186**, 316-343
776 Gaschnig R.M., Rudnick R.L., McDonough W. (2015) Standard addition ICP-MS
777 characterization of selected chalcophile and siderophile elements (Ga, Ge, Mo, Ag, Cd, In,
778 Sn, Sb, W, Tl, and Bi) in USGS whole-rock standard reference materials, Geostan. Geoanal.
779 Res. **39**, 371-379

780 Gaschnig R.M., Rudnick R.L., McDonough W.F., Kaufman A.J., Hu Z., Gao S. (2014) – Onset
781 of oxidative weathering of continents recorded in the geochemistry of ancient glacial
782 diamictites, *Earth Planet Sci. Lett.* **408,** 87-99
783 Gaschnig R.M., Vervoort J.D., Lewis R.S., Tikoff B. (2011) Isotopic evolution of the Idaho
784 Batholith and Challis Intrusive Province, Northern US Cordillera, *J. Petrol.* **52**, 12, 2397-
785 2429
786 Goldschmidt V.M. (1937) The principles of distribution of chemical elements in minerals and
787 rocks, Hugo Müller Lecture, Chemical Society
788 Greaney A.T., Rudnick R.L., Helz R.T., Gaschnig R.M., Piccoli P.M., Ash R.D. (2017) The
789 behavior of chalcophile elements during magmatic differentiation as observed in Kilauea Iki
790 Lava Lake, Hawaii, *Geochim. Cosmochim. Acta* **210**, 71-96
791 Greber N.D., Mader U., Nagler T.F. (2015) Experimental dissolution of molybdenum-sulphides
792 at low oxygen concentrations: A first order approximation of late Archean atmospheric
793 conditions, Earth Space Sci. **5**, 173-180
794 Greber N.D., Puchtel I.S., Nagler T.F., Mezger K. (2015) Komatiites constrain molybdenum
795 isotope composition of the Earth's mantle, *Earth Planet. Sci. Lett* **421**, 129-138
796 Gregory D.D., Lyons T.W., Large R.L., Jiang G., Stepanov A.S., Diamond C.W., Figueroa M.C.,
797 Olin P. (2017) Whole rock and discrete pyrite geochemistry as complementary tracers of
798 ancient ocean chemistry: An example from the Neoproterozoic Doushantuo Formation,
799 China, *Geochim. Cosmochim. Acta*, **216**, 201-222
800 Hannah J.L, Stein H.J., Wieser M.E., de Laeter J.R., Varner M.D. (2007) Molybdenum isotope
801 variations in molybdenite: Vapor transport and Rayleigh fractionation of Mo, *Geology* **35**,
802 703-706

803 Hawkesworth C.J., Bickle M.J., Gledhill A.R., Wilson J.F., Orpen J.L. (1979) A 2.9 Ga event in
804 the Rhodesian Archaean. *Earth Planet Sci Lett* **43**, 285–297
805 Helz G.R., Miller C.V., Charnock J.M., Mosselmans J.F.W., Pattrick R.A.D, Garner C.D.,
806 Vaughan D.J. (1996) Mechanism of molybdenum removal from the sea and its
807 concentration in black shales: EXAFS evidence, *Geochim. Cosmochim. Acta*, **60**, 19, 3631-
808 3642
809 Herrmann W. and Berry R.F. (2002) MINSQ – a least squares spreadsheet method for
810 calculating mineral proportions from whole rock major element analyses, *Geochemistry:*
811 *Exploration, Environment, Analysis* **2**, 361-368
812 Holzheid A., Borisov A., and Palme H. (1994). The effect of oxygen fugacity and temperature on
813 solubilities of nickel, cobalt, and molybdenum in silicate melts. *Geochim. Cosmochim.*
814 *Acta* **58** (8), 1975-1981
815 Jenner F.E. and O'Neill H.S.C (2012) Analysis of 60 elements in 616 ocean floor basaltic
816 glasses, *Geochem. Geophys. Geosyst.* **13** (1), 1-11
817 Jenner F.E. (2017) Cumulate causes for the low contents of sulfide-loving elements in the
818 continental crust, Nature Geoscience **10**, 524-529
819 Kasting J.F. (2014) Modeling the Archean Atmosphere and Climate, *Treatise on Geochemistry*,
820 2nd Edition, 157-173
821 König S., Wille M., Voegelin A., Schoenberg R. (2016) Molybdenum isotope systematics in
822 subduction zones, *Earth Planet. Sci. Lett.* **447**, 95-102
823 Kröner A., Byerly G.R., Lowe D.R. (1991) Chronology of early Archaean granite-greenstone
824 evolution in the Barberton Mountainland, South Africa, based on precise dating by single
825 zircon evaporation, *Earth Planet. Sci. Lett*. **103**, 41-54

826 Kuroda P.K. and Sandell E.B. (1954) Geochemistry of molybdenum, *Geochim. Cosmochim.*
827 *Acta*, **6**, 35-63
828 Liang Y., Halliday A.N., Siebert C., Fitton J.G., Burton K.W., Wang K., Harvey J. (2017)
829 Molybdenum isotope fractionation in the mantle, *Geochim. Cosmochim. Acta* **199**, 91-111
830 Lodders K. and Palme H. (1991) On the chalcophile character of molybdenum; determination of
831 sulfide/silicate partition coefficients of Mo and W, *Earth Planet. Sci. Lett.* **103**, 311-324
832 Luais B. and Hawkesworth C.J. (1994) The generation of continental crust: An integrated study
833 of crust-forming processes in the Archaean of Zimbabwe, *J. Petrol.* **35**, 43-93
834 Luais B. and Hawkesworth C.J. (2002) Pb isotope variations in the Archean and possible links to
835 the sources of certain Mesozoic-Recent basalts. In Fowler, C.M.R., Ebinger, C.J.
836 &.Hawkesworth , C.J. (eds.), *The Early Earth: Physical, Chemical and Biological*
837 *Development*. Geological Society, London, Special Publications **199**, 105–124
838 Lyons T.W., Reinhard C.T., Planavsky N.J. (2014) The rise of oxygen in Earth's early ocean and
839 atmosphere, *Nature*, **506**, 307-215
840 Ludington S., and Plumlee G.S. (2009) Climax-type porphyry molybdenum deposits: U.S.
841 Geological Survey Open-File Report 2009–1215, 1-16
842 Marks M.A., Coulson I.M., Schilling J., Jacob D.E., Schmitt A.K., Markl G. (2008) The effect of
843 titanite and other HFSE-rich mineral (Ti-bearing andradite, zircon, eudialyte) fractionation
844 on the geochemical evolution of silicate melts, *Chem. Geol.* **257**, 153-172
845 McDonough W.F. and Sun S.s (1995) The composition of the Earth, *Chem. Geol.* **120**, 223-253
846 Miller C.A., Peuker-Ehrenbrink B., Walker B.D., Marcantonio F. (2011) Re-assessing the
847 surface cycling of molybdenum and rhenium, *Geochim. Cosmochim. Acta*, **675**, 7146-7179

848 Moyen J.F., Stevens G., Kisters A.F.M., Belcher R.W. (2007) TTG plutons of the Barberton
849 Granitoid-Greenstone Terrain, South Africa, *Precambrian Ophiolites and Related Rocks,*
850 *Develop. Precamb. Geol*. **15**, 1-62
851 Newsom H.E. and Palme H. (1984) The depletion of siderophile element sin the Earth's mantle:
852 new evidence from molybdenum and tungsten, *Earth Planet Sci. Lett.* **69**, 354-364
853 O'Neill H.S.C. and Eggins S.M. (2002) The effect of melt composition on trace element
854 partitioning; and experimental investigation of the activity coefficients of FeO, NiO, CoO,
855 MoO_2 and MoO_3 in silicate melts, *Chem. Geol.* **186**, 151-181
856 Palme H. and O'Neill H.S.C. (2004) Cosmochemical estimates of Mantle Composition, *Treatise*
857 *on Geochemistry*, 1st edition, 1-38
858 Paton C., Hellstrom J., Paul B., Woodhead J., Hergt J. (2011) Iolite: Freeware for the
859 visualisation and processing of mass spectrometric data, *J. Anal. Atom. Spectrom.* **26**, 2508-
860 2518
861 Patten, C., Barnes, S., Mathez, E.A., Jenner, F.E. (2013) Partition coefficients of chalcophile
862 elements between sulfide and silicate melts and the early crystallization history of sulfide
863 liquid: LA-ICP-MS analysis of MORB sulfide droplets, *Chem. Geol.* **358**, 170-188
864 Pettke T., Oberli F., Heinrich C.A. (2010) The magma and metal source of giant porphyry-type
865 ore deposits, based on lead isotope microanalysis of individual fluid inclusions, *Earth Planet*
866 *Sci. Lett.* **296**, 267-277
867 Rayner N.M., Sanborn-Barrie S., Young M.D., Whalen J.B. (2012) U-Pb ages of Archean
868 basement and Paleoproterozoic plutonic rocks, southern Cumberland Peninsula, eastern
869 Baffin Island, Nunavut, *Geological Survey of Canada, Current Research 2012-8*, 1-24

Rudnick R.L. and Gao S. (2014) Composition of the Continental Crust, *Treatise on Geochemistry*, 2nd Edition 1-45

Scott C., Lyons T.W., Bekker A., Shen Y., Poulton S.W., Chu X., Anbar A.D. (2008) Tracing the stepwise oxygenation of the Proterozoic ocean, *Nature* **452**, 456-459

Shannon R.D. (1976) Revised Effective Ionic Radii and Systematic Studies of Interatomic Distances in Halides and Chalcogenides, *Acta Cryst* **32**, 751-767

Siebert C., Nägler T.F., von Blanckenburg R., Kramers J.D. (2003) Molybdenum isotope records as a potential new proxy for paleoceanography, *Earth Planet Sci. Lett.* **211**, 159-171

Skora S., Freymuth H., Blundy J., Elliott T., Guillong M. (2017) An experimental study of the behaviour of cerium/molybdenum ratios during subduction: Implications for tracing the slab component in the Lesser Antilles and Mariana Arc, *Geochim. Cosmochim. Acta* **212**, 135-155

Stein, H.J., 1985, A lead, strontium, and sulfur isotope study of Laramide-Tertiary intrusions and mineralization in the Colorado Mineral Belt with emphasis on Climax-type porphyry molybdenum systems plus a summary of other newly acquired isotopic and rare earth element data [Ph.D. thesis] Chapel Hill, University of North Carolina, 493 p.

Sun W., Li C., Hao X., Ling M., Ireland T., Ding X., Fan W. (2016) Oceanic anoxic events, subduction style, and molybdenum mineralization, *Solid Earth Sciences* **1**, 64-73

Stüeken E.E., Buick R., Guy B.M., Koehler M.C. (2015) Isotopic evidence for biological nitrogen fixation by molybdenum-nitrogenase from 3.2 Gyr, *Nature* **520**, 666-669

Tang M., Chen K., Rudnick R.L. (2016) Archean upper crust transition from mafic to felsic marks the onset of plate tectonics, *Science* **351**, 372-375

908 Taylor S.R. and McLennan S. (1985) The continental crust: Its composition and evolution,
909 Blackwell, Malden, MA
910 Turekian K.K. and Bertine K.K (1971) Deposition of molybdenum and uranium along the major
911 ocean ridge systems, *Nature*, **229**, 250-251
912 United States Geological Survey (2009) Mineral commodity summaries 2009: U.S. Geological
913 Survey, 195 p.
914 Voegelin A.R., Pettke T., Greber N.D., von Niederhäusern B., Nägler T.F. (2014) Magma
915 differentiation fractionates Mo isotope ratios: Evidence from the Kos Plateau Tuff (Aegean
916 Arc), *Lithos* **190-191**, 440-448
917 Walker R.J. (2016) Siderophile elements in tracing planetary formation and evolution, *Geochem.*
918 *Perspect.* **5**, No. 1, 1-143
919 Westra G. and Keith S.B. (1981) Classification and Genesis of Stockwork Molybdenum
920 Deposits, *Econ. Geol.* **76**, 844-873
921 Whalen J.B., Sanborn-Barrie M., Young M. (2012) Geochemical data from Archean and
922 Paleoproterozoic plutonic and volcanic rocks of Cumberland Peninsula, eastern Baffin
923 Island, Nunavut, *Geol. Survey Canada Open File 6933*
924 Whalen J.B. Wodicka N., Taylor B.E., Jackson G.D. (2010) Cumberland batholith, Trans-
925 Hudson Orogen, Canada: Petrogenesis and Implications for Paleoproterozoic crustal and
926 orogenic processes, *Lithos* **117**, 99-118
927 Whalen J.B., Percival J.A., McNicoll V.J., Longstaffe F.J. (2003) Intra-oceanic production of
928 continental crust in a Th-depleted ca. 3.0 Ga arc complex, western Superior Province,
929 Canada, *Contrib. Mineral. Petrol*. **146**, 78-99

930 Whalen J.B., Percival J.A., McNicoll V.J., Longstaffe F.J. (2002) A mainly crustal origin for
931 tonalitic granitoid rocks, Superior Province, Canada: Implications for Late Archean
932 tectonomagmatic processes, *J. Petrol.* **43**, 8, 1551-1570
933 Whalen J.B., Anderson R.G., Struik L.C., Villeneuve M.E. (2001) Geochemistry and Nd
934 isotopes of the François Lake plutonic suite, Endako batholith: host and progenitor to the
935 Endako molybdenum camp, central British Columbia, *Can. J. Earth Sci.* **38**, 603–618
936 Willbold M., Hibbert K., Lai Y-J., Freymuth H., Hin R.C., Coath C., Vils F., Elliott T. (2016)
937 High-Precision Mass-Dependent Molybdenum Isotope Variations in Magmatic Rocks
938 Determined by Double-Spike MC-ICP-MS, Geostan. Geoanal. Res. **40**, 389-403
939 Willbold M. and Elliot T. (2017) Molybdenum isotope variations in magmatic rocks, *Chem.*
940 *Geol.* **449**, 253-268
941 Wille M., Nebel O., Pettke T., Vroon P.Z., Konig S., Schoenberg R. (2018) Molybdenum isotope
942 variations in calc-alkaline lavas from the Banda arc, Indonesia: Assessing the effect of
943 crystal fractionation in creating isotopically heavy continental crust, *Chem. Geol.* **485**, 1-13
944 Wille M., Kramers J.D., Nagler T.F., Beukes N.J., Schroder S., Meisel Th., Lacassie J.P.,
945 Voegelin A.R. (2007) Evidence for a gradual rise of oxygen between 2.6 and 2.5 Ga from
946 Mo isotopes and Re-PGE signatures in shales, *Geochim. Cosmochim. Acta*, **71**, 2417-2435
947 Williamson M.A. and Rimstidt J.D. (1994) The kinetics and electrochemical rate-determining
948 step of aqueous pyrite oxidation, *Geochim. Cosmochim. Acta* **58**, 5443-5454
949 Yang J., Siebert C., Barling J., Savage P., Liang Y., Halliday A. (2015) Absence of molybdenum
950 isotope fractionation during magmatic differentiation at Hekla volcano, Iceland, *Geochim.*
951 *Cosmochim. Acta* **162**, 126-136

952 Yang J., Barling J., Siebert C., Fietzke J., Stephens E., Halliday A.N. (2017) The molybdenum
953 isotopic compositions of I-, S-, and A-type granitic suites, *Geochim. Cosmochim. Acta* **205**,
954 168-186
955 Zack T., Kronz A., Foley S.F., Rivers T. (2002) Trace element abundances in rutiles from
956 eclogites and associated garnet mica schists, *Chem. Geol.* **184**, 97-122
957 Zajacz Z., Halter W.E., Pettke T., Guillong M. (2008) Determination of fluid/melt partition
958 coefficients by LA-ICPMS analysis of co-existing fluid and silicate melt inclusions:
959 Controls on element partitioning, *Geochim Cosmochim Acta*. **72**, 2169-2197
960 Zajacz Z., Candela P.A., Piccoli P.M. (2017) The partitioning of Cu, Au and Mo between liquid
961 and vapor at magmatic temperatures and its implications for the genesis of magmatic-
962 hydrothermal ore deposits, *Geochim Cosmochim Acta*. **207**, 81-101
963
964

Figure 1. Photomicrographs of sulfides targeted for laser ablation analysis. A) Immiscible sulfide bleb from the Kilauea Iki lava lake (KI67-3-76.2) showing needle-like exsolution textures. A second minute (≤1 μm diameter) sulfide is visible on the right. B) Pyrite from the Archean Superior province tonalite (WXP99-119). C) Small chalcopyrite inclusion (yellow) hosted in magnetite having ilmenite exsolution from a Mesozoic granite (10RMG005). D) Pyrite rimmed by magnetite from the Paleozoic Ellicott City Granodiorite (AG1401).

Figure 2. Box and whisker plots of Mo abundances in all the minerals analyzed. Minerals are arranged by their median [Mo], with the boxes representing 1st and 3rd quartiles and whiskers representing min and max values measured. Upper plot: Granitic minerals from the Zimbabwe craton, Superior Province, and Phanerozoic granitic rocks. Plagioclase, epidote, and chlorite analyses were often below the detection limits. Lower plot: Minerals in basaltic to intermediate lavas from Kilauea Iki (red; data from Greaney et al., 2017) and MORB (blue; glass data from Jenner and O'Neill, 2012, sulfide data from Patten et al., 2013).

Figure 3. Pie charts depicting the total Mo distribution in four samples selected to show variation in major host minerals. Mass balance is achieved in three of the samples depicted (a,b,c), but 82% of the whole-rock [Mo] is missing from sample d. Sample numbers: A) WXP99-123 B) AG1401 C) KI67-3-76.2 D) 10RMG005.

Figure 4. UCC normalized spider plots showing Mo behavior relative to LREE in granitic suites (and their associated mafic enclaves/gabbros in the Superior and Baffin Island samples), and modern basalts. The differentiation suites from Zimbabwe, Baffin Island, and Superior Province

are defined with a gradient color scale (note the SiO_2 range varies for each suite with black and purple representing mafic or intermediate samples). Dashed lines indicate that Mo was below the detection limit in that sample, so the detection limit is used as the [Mo] value (see Table 1). All data are normalized to the UCC (Rudnick and Gao, 2014). Baffin Island data, except for Mo abundances, come from Whalen et al. (2012). The Kilauea Iki field represents twenty samples (Greaney et al., 2017) and the MORB field represents ~600 glass samples from Jenner and O'Neill (2012), with the mean values for both datasets shown with a line.

Figure 5. Correlations between Mo/Ce and Nb/La in Archean and Proterozoic pluton suites. Samples are color coded based on SiO_2 content with red being the most felsic and purple/black being the least. The SiO_2 range varies between suites (see Table 1 and supplementary figures). The Zimbabwe data include only the Mashaba tonalite suite. Error bars represent 2σ external reproducibility, as determined by AGV measurements.

Figure 6. UCC normalized spider plots for individual pluton suites in the Barberton Greenstone Belt representing different stages of accretion and post-orogenic collapse. Dashed lines indicate Mo was below the DL in the sample, so the DL is used instead of Mo concentration. Black = Steynsdorp; Green = Eerstehoek, Theespruit, Doornhoek, Stolzburg; Blue = Badplaas; Red = Nelshoogte.

F**igure 7**. Correlations between (A) Mo and Ni and (B) Mo and Cr in the Barberton TTGs. Color scheme is the same as in figure 6; dashed symbols represent samples that contain less Mo than the detection limit (0.16 ~~μg/g~~~~ppm~~). Error bars represent 2σ.

Table 1. Samples analyzed for whole-rock (WR) [Mo] and in-situ [Mo]. SA = standard addition ICP-MS; LA = laser ablation ICP-MS; MB = mass balance attained? (yes or no). The SiO_2 (measured by the listed reference) and Mo values given are for the whole rock with 2σ representing internal error. Three samples were replicated by isotope dilution and those values are designated as "rep". Complete whole rock major and trace element data can be found in the online supplement.

Table 2. Secondary standards analyzed by laser ablation and standard addition. Concentrations are in µg/g~~ppm~~. LA = Laser ablation-ICP-MS and SA = Standard addition whole rock-ICP-MS. BHVO-1 and AGV-2 were measured during the same analytical session as data reported in Greaney et al. (2017). Complete analytical methods can be found in the supplementary information.

Table 3. Mean Mo concentrations in all minerals analyzed (including granitic rocks and basalts). 2σ represents two standard deviations of the mean of repeated analyses. Analyses of sulfides, quartz, amphibole, K-feldspar, zircon, plagioclase, and epidote were occasionally below the detection limits (~0.01 µg/g~~ppm~~), so the detection limit of 0.01 µg/g~~ppm~~ was included in place of those analyses when calculating the mean concentration. Therefore, these data may be skewed to slightly higher values than actually present in the mineral.

Table 1

Sample	Unit/ Pluton	Age, Ga	Rock type	Analysis	MB	SiO_2	Mo (µg/g)
Barberton							
NLG1	Nelshoogte	3.24-3.23	TTG	SA		70.1	0.34
NLG14	Nelshoogte	3.24-3.23	TTG	SA		NA	0.38
NLG15	Nelshoogte	3.24-3.23	TTG	SA		63.1	0.48
NLG25A	Nelshoogte	3.24-3.23	TTG	SA		71.1	0.32
BDP5A	Badplaas	3.29-3.24	TTG	SA		70.5	<0.16
BDP5C	Badplaas	3.29-3.24	tonalite dyke	SA		72.8	0.17
BDP8A	Badplaas	3.29-3.24	TTG	SA		74	0.18
EHK1	Eerstehoek	3.46-3.42	TTG	SA		72.4	<0.16
TH4A	Theespruit	3.46-3.42	TTG	SA		70.3	0.20
DNK1	Doornhoek	3.46-3.42	TTG	SA		74	0.23
STZ1	Stolzburg	3.46-3.42	TTG	SA		70.7	0.48
STZ17	Stolzburg	3.46-3.42	TTG	SA		71.6	0.34
STY1	Steynsdorp	3.55-3.49	TTG	SA		65.7	0.16
STY1 rep							0.14
STY3A	Steynsdorp	3.55-3.49	TTG	SA		72.9	0.16
STY4B	Steynsdorp	3.55-3.49	TTG	SA		75.1	<0.16
Zimbabwe							
Zb89-53	Chibi	2.7-2.6	granite	SA, LA	no	72	0.84
Zb89-57	Chibi	2.7-2.6	granite	SA		74.8	0.26
ZB89-10	Mashaba I	2.9	tonalite	SA, LA	no	71	0.25
ZB89-10 rep							0.13
ZB89-11	Mashaba I	2.9	tonalite	SA		67.3	0.07
Zb89-12	Mashaba I	2.9	tonalite	SA		69.4	0.14
Zb89-13	Mashaba I	2.9	tonalite	SA, LA	yes	68.5	0.20
Zb89-15	Mashaba I	2.9	tonalite	SA, LA	yes	70.5	0.13
Zb89-46	Mashaba I	2.9	tonalite	SA		70.1	0.07
Rh75-Mt7	Mashaba I	2.9	tonalite	SA		71.2	0.05
Superior							
WXP99-119	N. Caribou	2.999	tonalite	SA	no	63.7	0.16
WXP99-123	N. Caribou	2.999	tonalite	SA, LA	yes	62.6	0.14
WXP99-138	N. Caribou	2.999	quartz diorite	SA	no	61.7	0.21
WXP99-176	N. Caribou	3.006	trondhjemite	SA, LA		72.1	0.32
WXP99-129	N. Caribou	2.999	tonalite	SA		62.5	nd
WXP 99-139	N. Caribou	NA	quartz diorite	SA		63.8	<0.10
WXP 99-143	N. Caribou	NA	quartz diorite	SA		60.7	<0.10
WXP 99-143 rep							0.11
WXP 99-145	N. Caribou	2.992	gabbro enclave	SA		49.3	0.90
PBA99-2064c	N. Caribou	NA	gabbro enclave	SA		46.1	<0.10
PBA99-2072c	N. Caribou	NA	amph-lite encl.	SA		50.1	0.13
PBA99-2072e	N. Caribou	NA	pyx-ite encl.	SA		45.2	0.17
PBA97-23	C. Wabigoon	2.72-2.71	granite	SA, LA	yes	71.3	0.32
PBA97-319	C. Wabigoon	2.72-2.71	granodiorite	SA		69.6	0.17
Baffin Island							

Table 2

secondary standard	analysis	Mo (reported)	Mo 95 measured	2s	Mo 97 measured	2s	Mo 98 measured	2s	n
BHVO-2g	LA	3.8	4.09	0.86	4.07	1.15	4.03	1.16	89
NIST 612	LA	37.4	43.6	16.2	40.4	14.0	44.1	7.89	8
JB sulfide	LA	2.55	2.44	0.30	2.45	0.69	2.44	0.20	8
BHVO-1	SA	1.1*	1.17	0.34	1.19	0.33	1.17	0.34	8
AGV-2	SA	1.93*	1.94	0.13	1.93	0.1	1.92	0.07	5

** values from Gaschnig et al., 2015*

Table 3

	Titanite	Niobite	Magnetite	OIB Glass	Ilmenite	Sulfides	Rutile	Garnet
Mo (µg/g)	15.9	9.83	5.83	4.83	4.09	1.44	0.95	0.33
2σ	27.2	n/a	17.5	5.58	11.2	4.09	0.86	0.09
n	59	1	36	101	53	78	10	12
	Olivine	**Muscovite**	**Quartz**	**Hornblende**	**K-feldspar**	**Augite**	**Zircon**	**Plagioclase**
Mo (µg/g)	0.10	0.08	0.05	0.04	0.03	0.02	0.02	≤0.01
2σ	0.15	0.13	0.06	0.10	0.08	0.02	0.03	0.03
n	5	9	25	36	24	5	21	37

Figure 1

Click here to download high resolution image

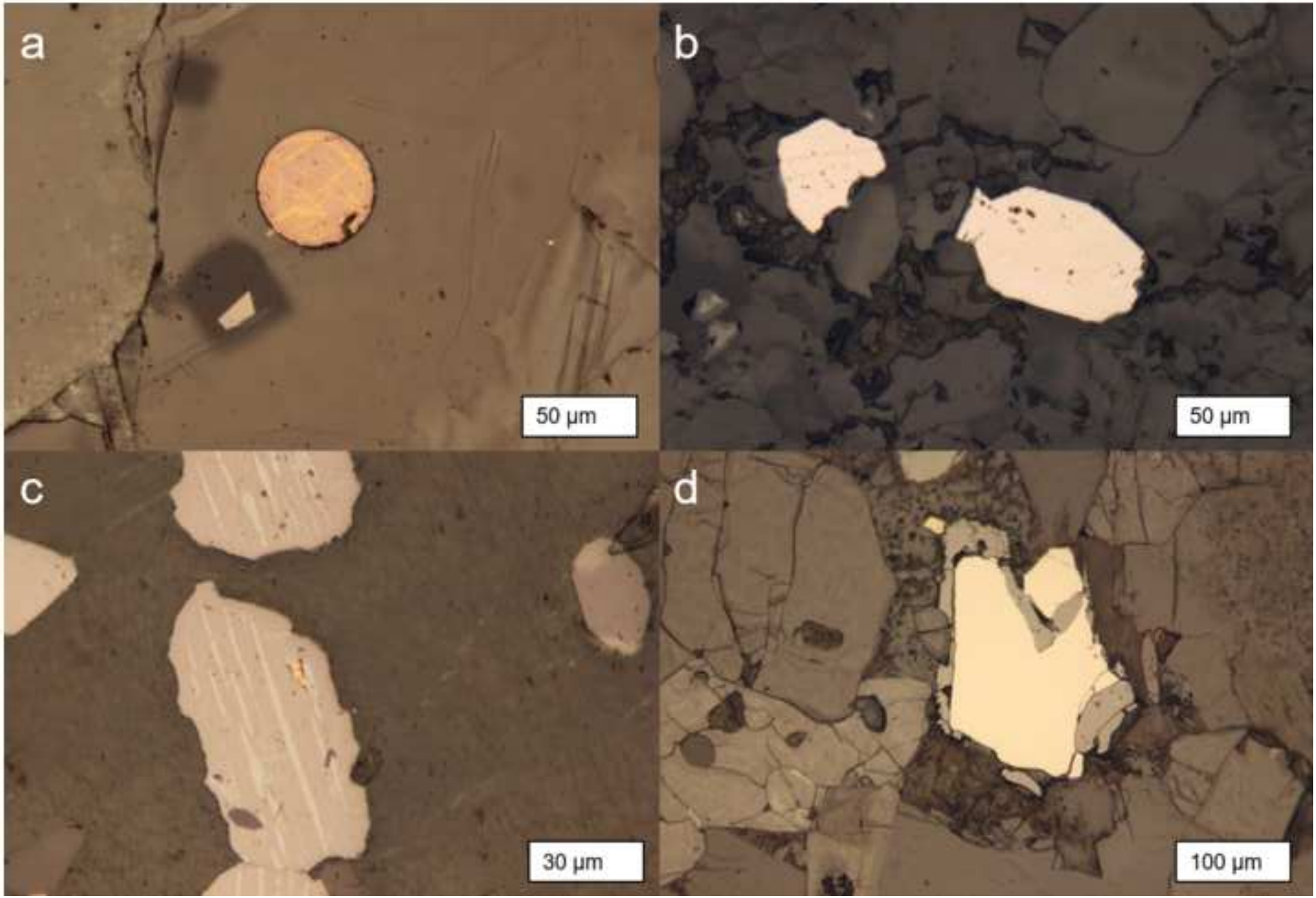

Figure 2

Click here to download high resolution image

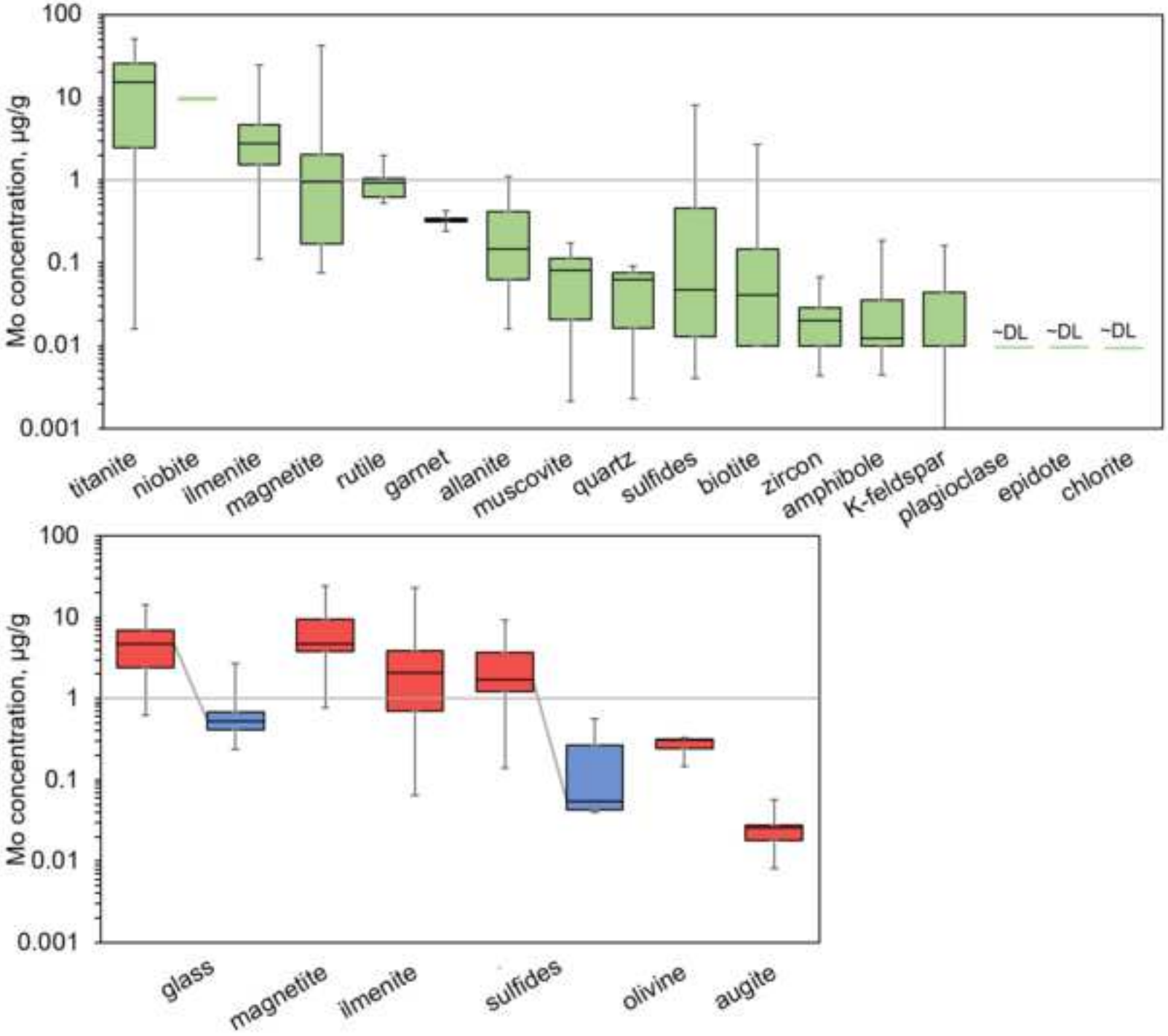

Figure 3

Click here to download high resolution image

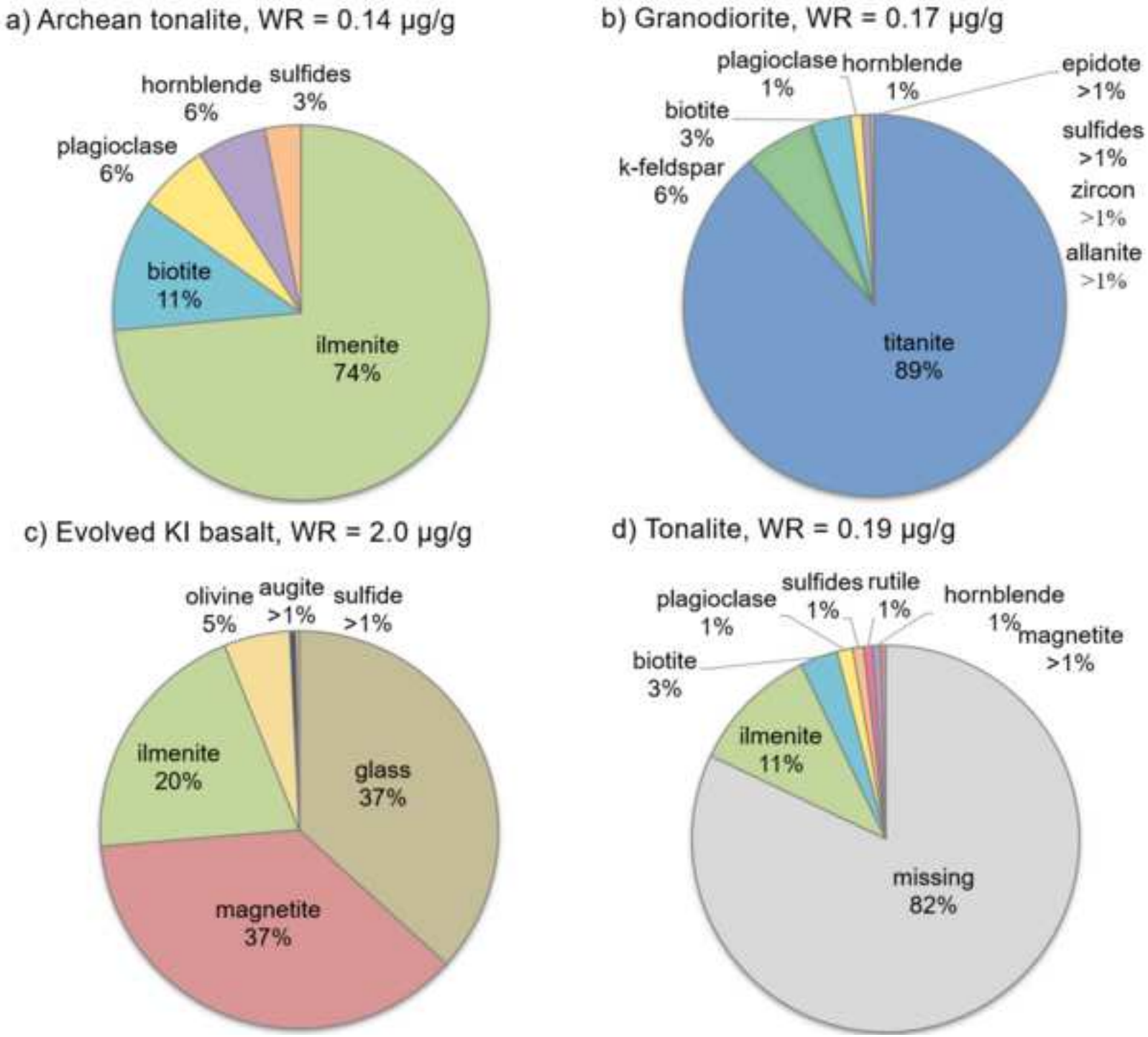

Figure 4

Click here to download high resolution image

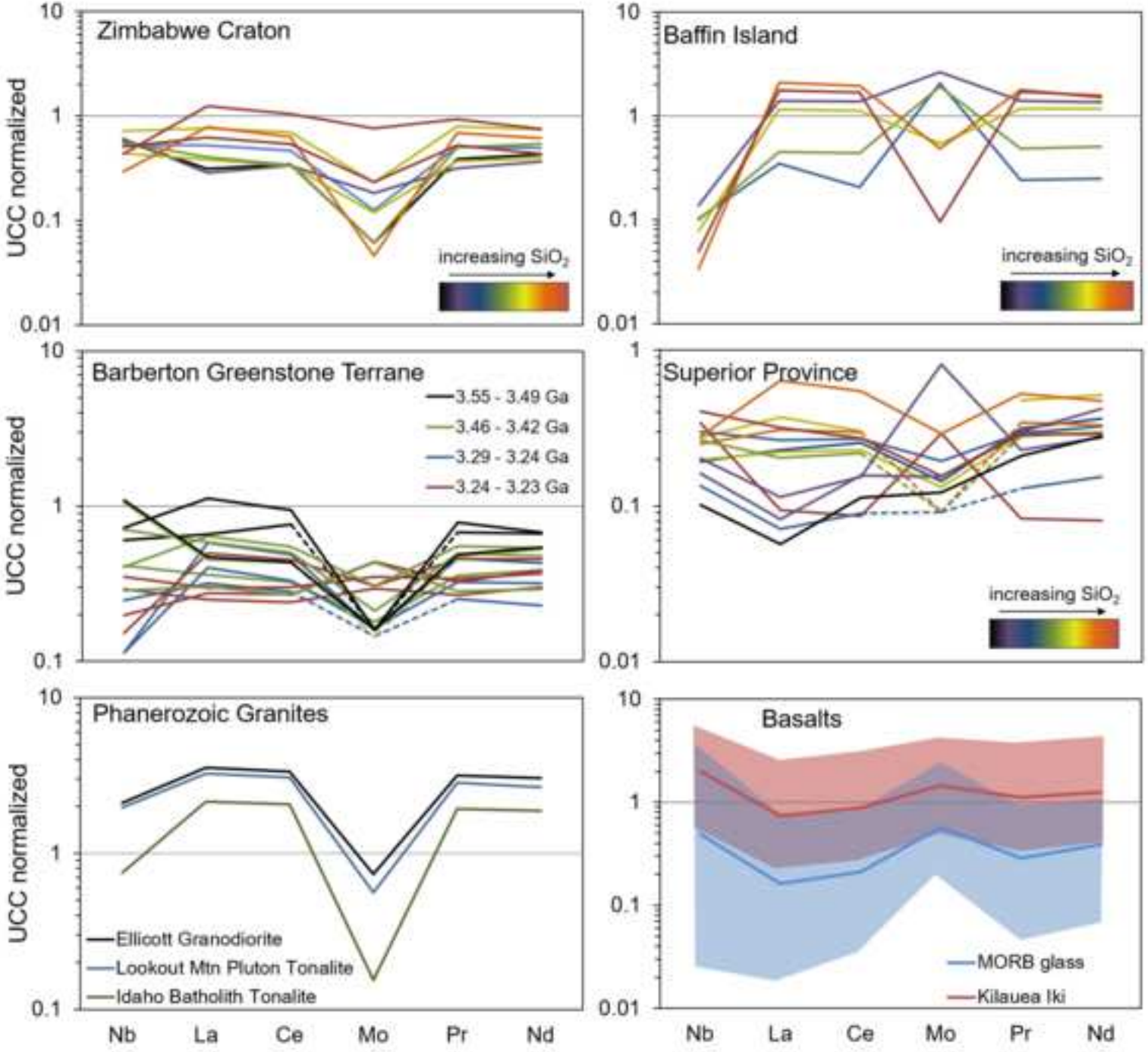

Figure 5

Click here to download high resolution image

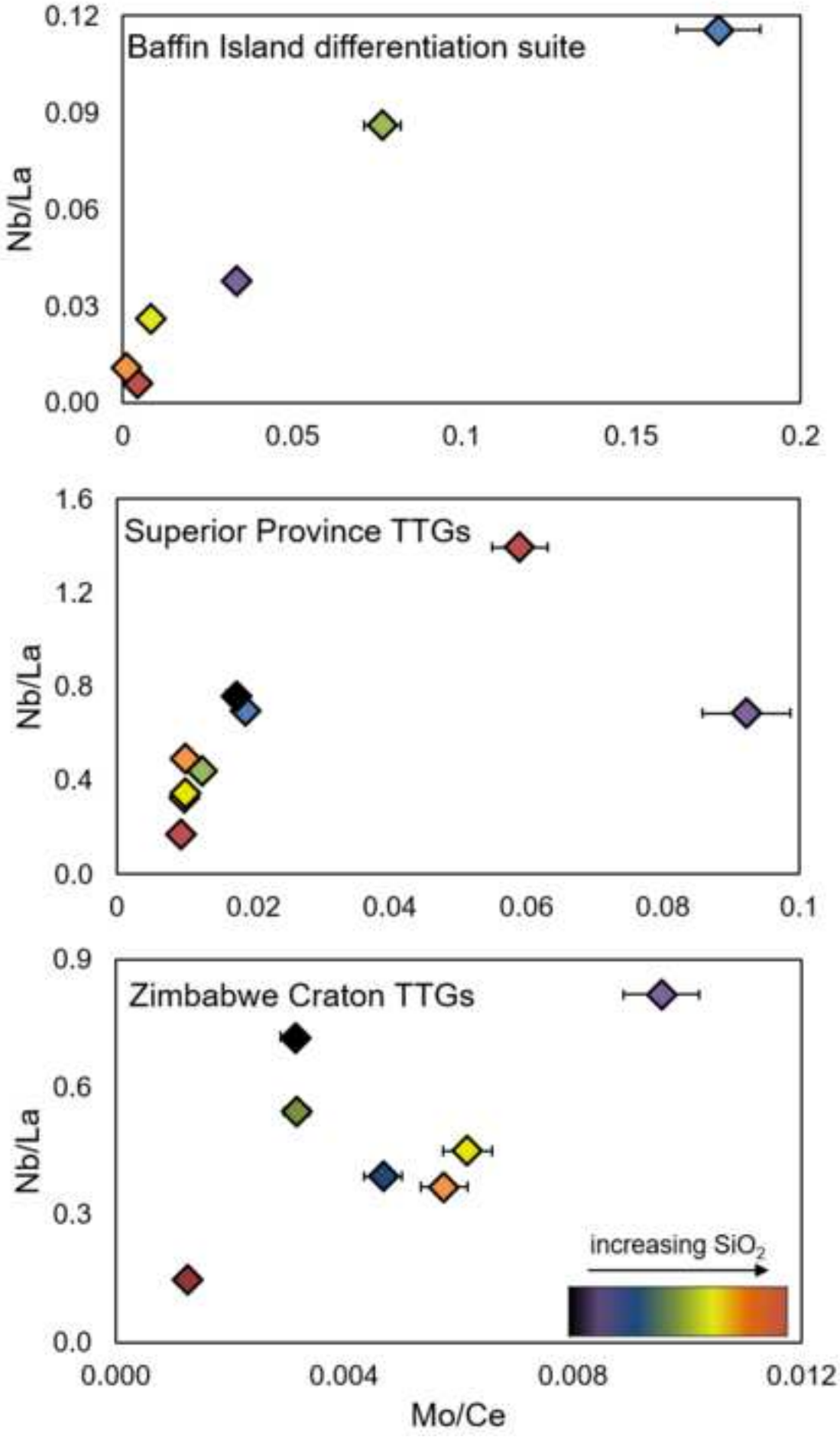

Figure 6

Click here to download high resolution image

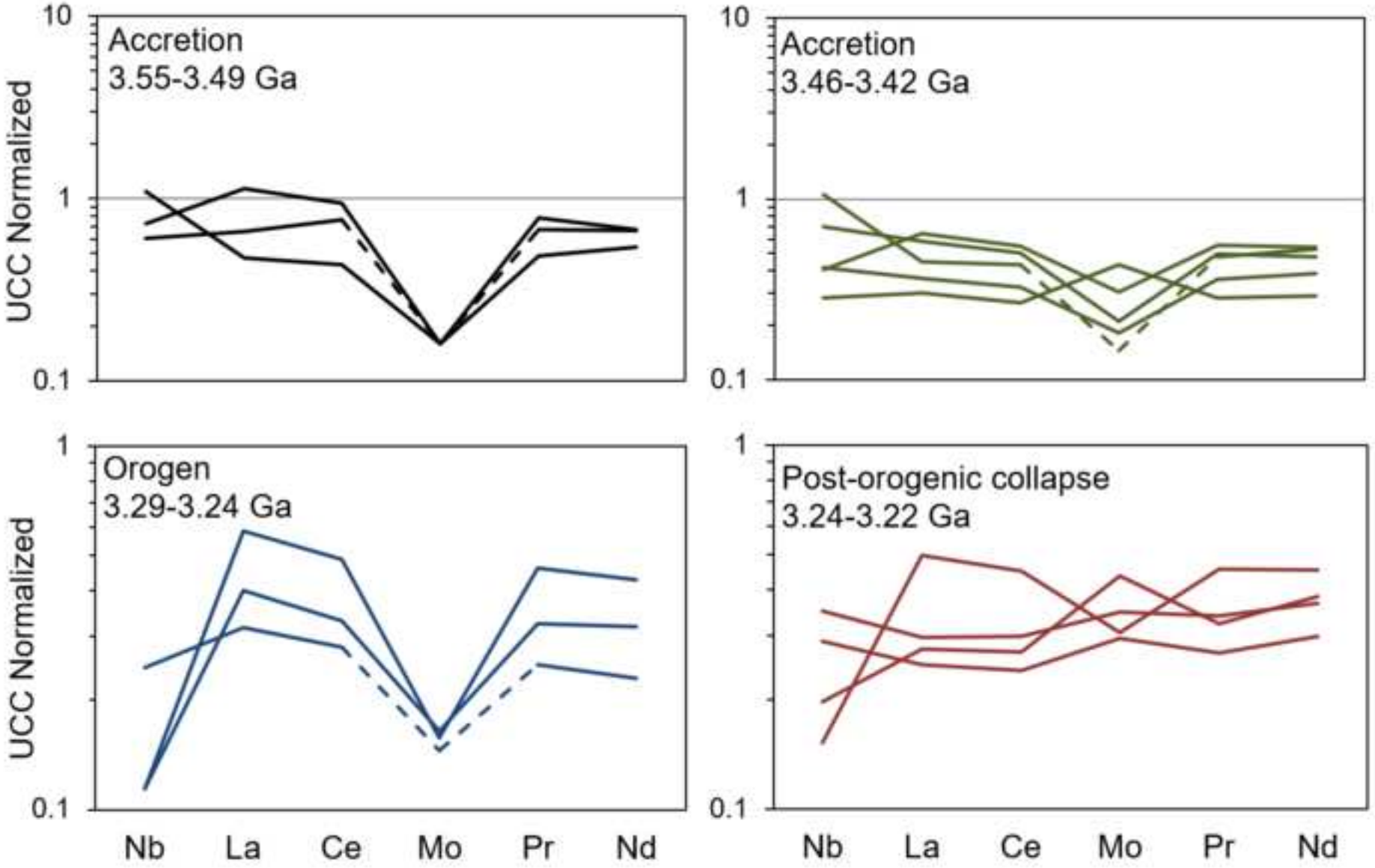

Figure 7

Click here to download high resolution image

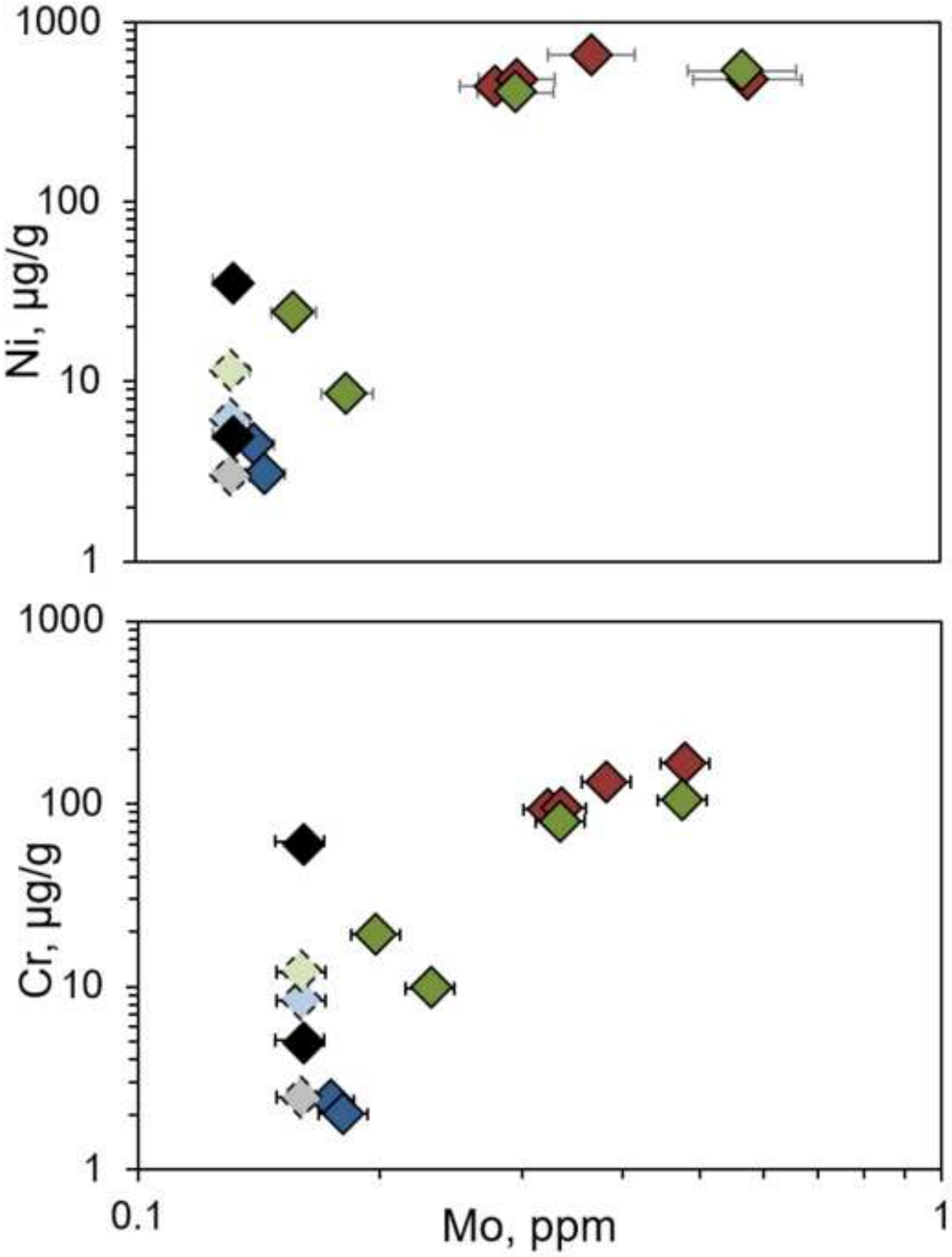

Supplementary Table

Click here to download Appendix: Whole Rock Data - supplement.xlsx

Appendix

Click here to download Appendix: Greaney et al. Supplement revised23.docx